The Meridional Flow of Source-Driven Abyssal Currents in a Stratified Basin with Topography. Part I: Model Development and Dynamical Properties

GORDON E. SWATERS

Applied Mathematics Institute, Department of Mathematical and Statistical Sciences, and Institute for Geophysical Research, University of Alberta, Edmonton, Alberta, Canada

(Manuscript received 15 February 2005, in final form 3 August 2005)

ABSTRACT

The equatorward flow of source-driven grounded deep western boundary currents within a stratified basin with variable topography is examined. The model is the two-layer quasigeostrophic (QG) equations, describing the overlying ocean, coupled to the finite-amplitude planetary geostrophic (PG) equations, describing the abyssal layer, on a midlatitude β plane. The model retains subapproximations such as classical Stommel–Arons theory, the Nof abyssal dynamical balance, the so-called planetary shock wave balance (describing the finite-amplitude β-induced westward propagation of abyssal anomalies), and baroclinic instability. The abyssal height field can possess groundings. In the reduced gravity limit, a new nonlinear steady-state balance is identified that connects source-driven equatorward abyssal flow (as predicted by Stommel–Arons theory) and the inertial topographically steered deep flow described by Nof dynamics. This model is solved explicitly, and the meridional structure of the predicted grounded abyssal flow is described. In the fully baroclinic limit, a variational principle is established and is exploited to obtain general stability conditions for meridional abyssal flow over variable topography on a β plane. The baroclinic coupling of the PG abyssal layer with the QG overlying ocean eliminates the ultraviolet catastrophe known to occur in inviscid PG reduced gravity models. The baroclinic instability problem for a constant-velocity meridional abyssal current flowing over sloping topography with β present is solved and the stability characteristics are described.

1. Introduction

In a source region of deep water formation, the Sverdrup vorticity balance predicts equatorward abyssal flow (Stommel and Arons 1960). Away from the source region, Stommel–Arons theory cannot infer the flow direction of abyssal currents. However, many abyssal currents are characterized by the isopycnal field being grounded against sloping topography [e.g., the deep western boundary undercurrent in the North Atlantic (Richardson 1977) and the deep water replacement current in the Strait of Georgia (LeBlond et al. 1991; Masson 2002)] and the flow being in geostrophic balance. As shown by Nof (1983), a fully grounded abyssal water mass lying over sloping topography flows, in the fully nonlinear but reduced gravity dynamical limit, nondispersively and steadily in the along-slope direction, irrespective of the specific height or vorticity field within the abyssal water mass.

These two results provide a dynamical scenario for the initiation and maintenance of source-driven grounded abyssal flow. That is, in high latitude regions where deep water is produced (often over sloping topography), the Sverdrup vorticity balance initiates equatorward flow. Once produced, this water mass can become grounded and geostrophically adjusted, maintaining a Nof balance that permits sustained basin-scale meridional quasi-steady and coherent abyssal flow. Of course, this picture leaves out important dynamics such as diabatic and planetary effects, baroclinicity, instability, topographic separation and mixing. In addition, such a scenario cannot explain cross-equatorial abyssal currents where the assumptions of geostrophically balanced flow must break down (see, e.g., Nof and Borisov 1998; Edwards and Pedlosky 1998a,b; Stephens and Marshall 2000; Choboter and Swaters 2003, 2004), the superinertial instability associated with frictional super-

Corresponding author address: Gordon E. Swaters, Department of Mathematical and Statistical Sciences, University of Alberta, Edmonton, AB, T6G 2G1, Canada.
E-mail: gordon.swaters@ualberta.ca

critical abyssal overflows (Swaters 2003) or the relatively rapid barotropic instability that can occur in the overlying water column as a result of spinup associated with baroclinic stretching (Sutherland et al. 2004).

The principal purpose of the present contribution is to present a baroclinic model that describes the formation and development of grounded abyssal currents as a process that begins as a source-driven Stommel–Arons flow and then transitions to a Nof flow as the abyssal water mass flows equatorward. In particular, the subinertial evolution and equatorward flow of source-driven grounded abyssal currents over sloping topography and their baroclinic interaction with the overlying ocean on a midlatitude β plane is described. The importance of this process in understanding the planetary-scale overturning of the oceans, and hence climate dynamics, is obvious. However, this paper is oriented more toward describing the mesoscale dynamics, kinematic features, and baroclinic development, and the basin-scale characteristics of deep grounded abyssal currents, that these processes imply.

The plan of this paper is as follows. In section 2, the model is introduced and estimates of the magnitude of the many physical parameters are given. In the appendix, it is shown how the model can be obtained via a subinertial small-slope asymptotic reduction of the three-layer shallow water equations.

Section 3 describes various dynamical sublimits that exist within the abyssal layer equation. It is shown that the model recovers the Stommel–Arons theory for the equatorward flow of a source-driven abyssal water mass (Stommel and Arons 1960), the nondispersive topographically steered inertial flow of a grounded abyssal water mass (Nof 1983), and the finite-amplitude β-induced westward propagation of abyssal water masses associated with the so-called planetary shock wave balance introduced by Anderson and Killworth (1979) and examined later by Johnson and Willmott (1981), in the continuously stratified context, and by Dewar (1987a) and Wright and Willmott (1992), in the layered context.

In addition, in section 3, new hybrid nonlinear reduced-gravity steady-state balance is introduced that bridges both Stommel–Arons and Nof dynamics. This model is explicitly solved to determine the meridional structure of an abyssal current that possesses cross-slope groundings (like that shown in Fig. 1). The theory predicts the equatorward thinning of the abyssal layer height (although the meridional transport is constant, i.e., the equatorward speed of the abyssal current increases in the equatorward direction) because of the conservation of PG potential vorticity. The influence of β is to (slightly) orient the pathlines in the northeast to southwest direction, that is, there is a cross-slope component in the abyssal velocity field. The solution does not correspond to a simple parallel shear flow.

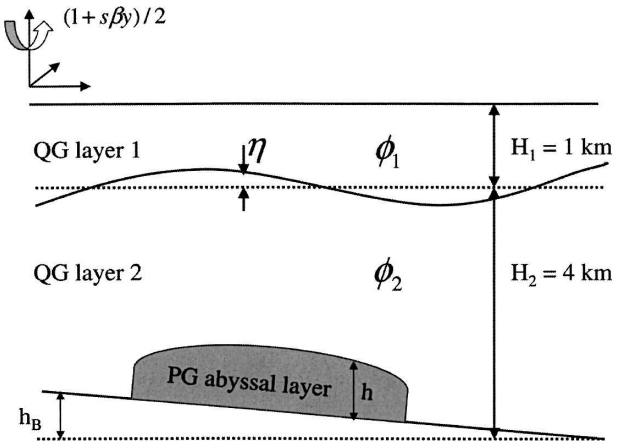

FIG. 1. Model geometry used in this paper.

In section 4, the baroclinic instability characteristics of the model are examined. A variational principle is introduced for the baroclinic extension of all inertial solutions to the hybrid Stommel–Arons–Nof model. This variational principle is exploited to establish (modal and nonmodal) sufficient stability and necessary instability conditions. The linear baroclinic instability problem is solved for a constant-velocity abyssal current with β and sloping topography present. The most unstable mode, for typical parameter values, corresponds to an equatorward (or along-slope) propagating topographic Rossby wave with a wavelength on the order of 90 km, a period of about 38 days (the phase speed is about 3 cm s^{-1}) and an *e*-folding amplification time of about 6 days. In section 5 a summary is given, as well a brief description of future work.

2. Model equations

The model is an amalgamation, with the inclusion of variable topography and mass conserving up and downwelling, of the two-layer quasigeostrophic (QG) (i.e., Phillips) model used, for example, by Holland (1978) to investigate the baroclinic evolution of the wind driven circulation and the QG/planetary geostrophic (PG) abyssal current model of Swaters (1991) describing the baroclinic instability of grounded abyssal flow on sloping topography. A continuously stratified version of the model is described by Poulin and Swaters (1999) and Reszka et al. (2002).

Assuming a Boussinesq, rigid-lid approximation with wind stress, horizontal and bottom friction, variable topography, and mass conserving up- or downwelling, the

nondimensional model, in standard notation (see, e.g., Pedlosky 1987), can be written in the form

$$[\partial_t + J(\phi_1, \cdot)][\Delta\phi_1 - F_1(\phi_1 - \phi_2) + \beta y] = \Upsilon\nabla \times \boldsymbol{\tau} + \frac{F_1 Q}{F_1 + F_2} + \frac{\Delta^2\phi_1}{R_e}, \quad (2.1)$$

$$[\partial_t + J(\phi_2, \cdot)][\Delta\phi_2 - F_2(\phi_2 - \phi_1) + h + h_B + \beta y] = -r_2\Delta\phi_2 + \frac{F_1 Q}{F_1 + F_2} + \frac{\Delta^2\phi_2}{R_e}, \quad \text{and} \quad (2.2)$$

$$h_t + J\left(h + \phi_2 + h_B, \frac{h}{1 + s\beta y}\right) = Q + r_3\Delta(\phi_2 + h_B + h), \quad (2.3)$$

with the auxiliary diagnostic relations

$$\mathbf{u}_{1,2} = \mathbf{e}_3 \times \nabla\phi_{1,2}, \qquad \mathbf{u}_3 = \frac{\mathbf{e}_3 \times \nabla(\phi_2 + h_B + h)}{1 + s\beta y},$$
$$p = \phi_2 + h_B + h, \quad \text{and} \quad \eta = \phi_2 - \phi_1, \quad (2.4)$$

with $J(A, B) = A_x B_y - A_y B_x$, and where the 1, 2, or 3 subscript on a physical variable refers to the upper, middle, and abyssal layer, respectively; alphabetical subscripts (unless otherwise noted) indicate partial differentiation, $\mathbf{u}_{1,2,3} = (u_{1,2,3}, v_{1,2,3})$, $\nabla = (\partial_x, \partial_y)$, $\Delta = \nabla \cdot \nabla$, h_B is the height of the topography, h is the height of the abyssal layer relative to h_B, η is the deflection (measured positively upward) of the interface between the two QG layers from its equilibrium position, $\boldsymbol{\tau}$ is the wind stress, and Q is the down- or upwelling term, respectively. The dynamic pressures in the upper two layers is given by $\phi_{1,2}$, and in the abyssal layer by p, respectively. The model geometry is shown in Fig. 1. Equations (2.4c) and (2.4d) express the continuity of total pressure across the deforming interfaces between the middle and abyssal layers and the upper and middle layers, respectively.

The dynamical parameters in the model are defined by

$$s = \frac{s^* L}{H_2}, \quad \beta = \frac{\beta^* L^2}{U_*}, \quad R_e = \frac{U_* L}{A_H}, \quad \Upsilon = \frac{\Upsilon^* L}{\rho_* H_1 U_*^2},$$
$$F_1 = \frac{g' H_2}{\tilde{g} H_1}, \quad F_2 = \frac{g'}{\tilde{g}}, \quad \text{and} \quad r_{2,3} = \frac{r^*_{2,3}}{s H_2}, \quad (2.5)$$

where $H_{1,2}$ are the constant reference layer thicknesses in the upper two layers, ρ_* is the reference Boussinesq density and $g' = (\rho_3 - \rho_2)g/\rho_* > 0$ and $\tilde{g} = (\rho_2 - \rho_1)g/\rho_* > 0$ where $\rho_{1,2,3}$ correspond to the constant density in each individual layer with $0 < \rho_1 < \rho_2 < \rho_3$, $L = \sqrt{g' H_2}/f_0$ (the internal deformation radius for the middle layer based on the density difference with the abyssal layer), $U_* = s^* g'/f_0$ (the Nof speed), $s^* \approx O(\nabla^* h_B^*)$ (a representative value for the topographic slope), f_0 is the reference Coriolis parameter, β^* is the northward gradient of the Coriolis parameter, and Υ^* is a typical value for the wind stress, respectively.

In addition, A_H is the upper layers' horizontal eddy coefficient and $r^*_{2,3}$ are bottom friction coefficients for the middle and abyssal layers, respectively. Ekman boundary layer theory (Pedlosky 1987) suggests that $r^*_{2,3} = H_{2,3}\sqrt{E^V_{2,3}}$, where $H_{2,3}$ are the vertical thickness scales and $E^V_{2,3}$ are the vertical Ekman numbers for the middle and abyssal layers, respectively. Accordingly, $r^*_{2,3}$ are the scale vertical thicknesses of the Ekman bottom boundary layer in the middle and abyssal layers, respectively.

The wind stress is explicitly distributed only over the upper layer and the upper layer does not have surface Ekman friction. The upper two layers have horizontal friction, but this has been neglected in the abyssal layer. The abyssal layer includes bottom friction. Though in geostrophic balance, the leading-order abyssal layer equations are not geostrophically degenerate and allow for finite-amplitude dynamic deflections in the abyssal layer height.

The upwelling/downwelling parameterization (the Q terms) is an adaptation of the interfacial mass flux model introduced by Dewar (1987b, 1988a,b) for warm rings and, subsequently, by Swaters and Flierl (1991) for abyssal cold domes. Physically, this parameterization models the upwelling or downwelling as an continuous conversion of abyssal layer water into (or from) overlying ocean water in such a way as to ensure that in the unforced, inviscid limit, the horizontal divergence of the barotropic mass flux is zero [see the appendix and Swaters and Flierl (1991)]. That is, whatever mass is accumulated into (or lost from) the abyssal layer is assumed to have been instantaneously gained from (or lost into) the upper two layers in proportion to the individual upper layer volume fractions. The net horizontal divergence of the barotropic mass transport is forced only by wind stress and bottom friction. In the unforced and inviscid limit, total volume is conserved with this upwelling/downwelling parameterization.

Although there is no thermodynamics in the model per se (so that there is no genuine heat or salinity transport), $Q > 0$ can be heuristically interpreted as a cooling of the overlying water column that leads to a downward mass flux resulting in the depletion of the overlying water mass and a corresponding increase in the volume of abyssal water. Similarly, $Q < 0$ can be heuristically interpreted as warming or freshening of the abyssal water mass that leads to an upward mass flux resulting in the depletion of the abyssal water mass and

a corresponding increase in the volume of upper ocean water.

The unforced, inviscid dynamics of the model is purely baroclinic. It is important to point out that the Dewar parameterization implies that the only densities allowed are the densities of the three layers in the model and that no intermediate density layer can be created and is dynamically appropriate for the discrete three-layer shallow-water-based model considered here. Similar parameterizations for the source terms for buoyancy-driven abyssal circulation in layered models (particularly in the reduced gravity approximation) have been introduced by, for example, Kawase (1987), Kawase and Straub (1991), Wright and Willmott (1992), Straub et al. (1993), and Willmott et al. (1996).

The model (2.1), (2.2), and (2.3) can be formally derived in a small Rossby number limit (i.e., $s \to 0$; see the appendix) of the three-layer shallow-water equations using the scaling arguments of Swaters and Flierl (1991), Swaters (1991), Poulin and Swaters (1999), and Reszka et al. (2002). Briefly, the abyssal-layer equations are scaled assuming that the dynamics is principally governed by a geostrophic balance between the down slope gravitational acceleration of the abyssal water mass and the Coriolis term. The upper layers are scaled assuming that the baroclinic stretching associated with deformations associated with the interface between the abyssal and middle layers is the same order of magnitude as the velocity field. This will imply that the appropriate length scale is the internal deformation radius associated with the middle layer and that time will be scaled advectively. All other variables are scaled assuming an underlying geostrophic balance to leading order.

From the point of view of the abyssal layer, this is an intermediate, or PG, dynamical limit [i.e., a subinertial regime in which the length scale is longer than the local internal deformation radius but shorter than the basin width, see Charney and Flierl (1981), Flierl (1984), Pedlosky (1984)]. The dominant nonlinearity is associated not with the flow acceleration but, rather with isopycnal steepening. This attribute allows the model to describe fully grounded finite-amplitude abyssal flow, in which the isopycnal field intersects the bottom, which is something QG theory cannot do. This scaling allows for strong baroclinic interaction between the abyssal current and overlying water column.

Since the ratio of the scale thickness of the abyssal layer (on the order of 100 m) to the scale thickness of the overlying ocean (on the order of 4000 m) is identical to the scaled slope parameter s [i.e., they are the same order of magnitude; see (2.5), (2.7), and (A.6)], the overlying ocean will have a finite deformation radius and, thus, baroclinic stretching associated with the interface between the upper two layers is retained in the QG potential vorticity. This fact has a very important implication in relation to the stability properties of the model. It is known that, in the purely inertial limit, the PG approximation exhibits an ultraviolet catastrophe in the linear instability problem [i.e., the most unstable wave mode occurs for an infinite wavenumber; see de Verdiere (1986)]. While the inclusion of Rayleigh damping can remove the ultraviolet catastrophe (Samelson and Vallis 1997), Swaters (1991) has shown that an inviscid baroclinic model, that couples an abyssal PG layer to an overlying QG layer (with its implicit finite deformation radius), also ensures that the most unstable mode occurs at a finite wavenumber. This property continues, of course, to hold if the overlying QG fluid is multilayered (as occurs here) or is continuously stratified (Poulin and Swaters 1999; Reszka et al. 2002).

Although there is considerable variability, typical basin-scale values of the physical parameters are

$$\begin{aligned} &\tilde{g} \simeq 9.5 \times 10^{-3}\ \mathrm{m\ s^{-2}}, \quad g' \simeq 4.8 \times 10^{-4}\ \mathrm{m\ s^{-2}}, \qquad s^* \simeq 5.6 \times 10^{-3}, \\ &\Upsilon^* \simeq 10^{-1}\ \mathrm{N\ m^{-2}}, \qquad H_1 \simeq 1\ \mathrm{km}, \qquad A_H \simeq 1.6 \times 10^{4}\ \mathrm{m^2\ s^{-1}}, \\ &H_2 \simeq 4\ \mathrm{km}, \qquad f_0 \simeq 9.35 \times 10^{-5}\ \mathrm{s^{-1}}, \quad \text{and} \quad \beta^* \simeq 1.6 \times 10^{-11}\ (\mathrm{ms})^{-1}, \end{aligned} \tag{2.6}$$

which implies that

$$\begin{aligned} &L \simeq 15\ \mathrm{km}, \quad U_* \simeq 3\mathrm{cm\ s^{-1}}, \qquad T \equiv \frac{Lf_0}{s^* g'} \simeq 6\ \mathrm{days}, \\ &(H_3, h_B^*) \equiv s^* L \simeq 84\ \mathrm{m}, \qquad \text{and} \qquad Q_* \equiv s^{*2} g'/f_0 \simeq 1.6 \times 10^{-2}\ \mathrm{cm\ s^{-1}}, \end{aligned} \tag{2.7}$$

where T, Q_*, H_3, and h_B^* are the formal scalings for the time, upwelling/downwelling mass exchange between the abyssal and the overlying ocean, abyssal layer thickness, and topographic height used in the derivation of

(2.1), (2.2), and (2.3), respectively. The rotational parameters f_0 and β^* have been evaluated at 40°N (the origin of the domain).

These scalings imply that the nondimensional parameters are about

$$s \simeq 0.02, \quad F_1 \simeq 0.2, \quad F_2 \simeq 0.05, \quad r_2 \simeq 0.08,$$
$$\beta \simeq 0.12, \quad R_e \simeq 1/35, \quad \Upsilon \simeq 1.62, \quad \text{and} \quad r_3 \simeq 0.001. \tag{2.8}$$

In this paper, the limit $\Upsilon = r_{2,3} = 0$ and $R_e \to \infty$ is examined (inviscid flow with no wind stress). In forthcoming contributions, which will focus on numerical simulations, Υ, Q, $r_{2,3}$, and R_e will be chosen so that the wind driven northward barotropic QG mass transport and zonal width of the western boundary current (i.e., the Gulf Stream), and the equatorward transport of the source-driven abyssal (i.e., deep western boundary) current is consistent with observations of the northwestern Atlantic Ocean.

The inclusion of the $O(s\beta)$ terms in (2.3) is, formally, an ad hoc approximation. Although the internal deformation associated with the middle layer is the length scale, which is the appropriate scaling for the $O(1)$ baroclinic coupling of interest here, the numerical simulations (which are described in Part II; see Swaters 2006) will be done in an 40° × 40°, or equivalently, an approximately 3660 km × 3660 km (or, nondimensionally, a 244 × 244) basin, that is, a domain that extends from 20° to 60°N. Over a meridional range this large, the $O(s\beta)$ terms in (2.3) make a not insignificant cumulative contribution and thus they will be retained even if, formally at least, the scaling suggests they can be ignored to leading order with respect to s. It is possible that a complete multiple scale asymptotic theory, similar to that described by Pedlosky (1984) for geostrophic flow, could be developed to make this ad hoc approximation rational.

Additionally, and perhaps most importantly, the inclusion of the $O(s\beta)$ terms allows that, in a steady, reduced gravity and flat bottom approximation, (2.3) reduces to the (vertically integrated) Sverdrup vorticity equation with a source term, which forms the basis of the Stommel and Arons (1960) theory for the equatorward flow of abyssal water. Thus, the classical Stommel–Arons theory is retained in a subapproximation of the model.

There are a variety of dynamical balances possible in models of this sort. Karsten and Swaters (1999, 2000) have given a general description of the differing dynamical balances possible as function of the underlying parameter space. It has been suggested by, for example, Jiang and Garwood (1996), Etling et al. (2000), and Jungclaus et al. (2001), that the instability seen in numerical simulations of abyssal overflows resembles the transition characteristics described by Swaters (1991, 1998). Choboter and Swaters (2000) have shown that aspects of the destabilization of dense flows on a sloping bottom observed in laboratory experiments (e.g., Lane-Serff and Baines 1998) can be described by the Swaters (1991) baroclinic instability theory.

Individual subapproximations of (2.1), (2.2), and (2.3) are very well known explicitly or in closely related form. The upper-layer equations in (2.1) and (2.2) are simply, of course, the Phillips two-layer model, with topography, friction, diabatic forcing, and wind stress present, which has been used extensively to examine various aspects of baroclinic instability on a β plane (see, e.g., Pedlosky 1987), the spinup of a stratified basin (Holland 1978) and the interaction of deep western boundary currents with the wind driven circulation (Katsman et al. 2001).

The abyssal equation in (2.3) is simply the planetary geostrophic equation for a single layer, with baroclinic coupling, topography, friction, and a mass source term, on a β plane (Pedlosky 1984). The PG approximation has been used widely to investigate aspects of abyssal and other long length scale flow (e.g., Stommel and Arons 1960; Anderson and Killworth 1979; Dewar 1987a; Kawase 1987; Kawase and Straub 1991; Straub et al. 1993; Wright and Willmott 1992; Rhines 1989; Speer et al. 1993; Stephens and Marshall 2000; among many others) and the thermohaline circulation (e.g., Edwards et al. 1998; Samelson and Vallis 1997; Samelson 1998, among many others). In particular, (2.3) can describe an abyssal current that possesses distinct incroppings or groundings (Speer and McCartney 1992) in its thickness or height, that is, $h = 0$ along a curve $\psi(x, y, t) = 0$. This is an important kinematic property of the cross-slope structure in deep western boundary undercurrents (that QG theory cannot reproduce; see, e.g., Katsman et al. 2001).

3. Theoretical properties

There are a number of subdynamical, or distinguished, limits in (2.3) such as the Nof balance describing topographically steered abyssal flow (Nof 1983), the Stommel–Arons Sverdrup vorticity balance describing the equatorward flow of an abyssal water mass created by a source (Stommel and Arons 1960), the planetary shock wave balance (Anderson and Killworth 1979; Johnson and Willmott 1981; Dewar 1987a; Wright and Willmott 1992; among others) describing the amplitude-β induced isopycnal steepening associated with the frontal geostrophic dynamical regime (Karsten and

Swaters 1999, 2000) and, finally, the coupling between the abyssal layer and the overlying ocean that can lead to baroclinic instability and mixing (Swaters 1991, 1998). Each of these processes plays an important role in determining aspects of the spatial and temporal structure of the abyssal currents modeled here. It is useful to briefly review these approximations, and a few other properties of the model, and their dynamical implications. The area-integrated energy for the model is given by

$$\mathcal{E} = \frac{1}{2}\int\int_{\Omega} \{F_2 \nabla\phi_1 \cdot \nabla\phi_1 + F_1[\nabla\phi_2 \cdot \nabla\phi_2 + (h + h_B)^2 - h_B^2] + F_1F_2(\phi_1 - \phi_2)^2\}\, dx\ dy, \tag{3.1}$$

where Ω is the fixed spatial horizontal domain. In the absence of wind forcing, interlayer mass exchange and dissipation (i.e., $\Upsilon = Q = r_{2,3} = 0$, $R_e \to \infty$), it follows that $d\mathcal{E}/dt = 0$. In the unforced situation, (2.1), (2.2), and (2.3) is an infinite-dimensional Hamiltonian dynamical system (see, e.g., Swaters 1993, 2000), in which $\mathcal{E}$ will be the Hamiltonian functional, and it is possible to establish a variational principle for steady solutions for the model and use these to examine general stability criterion (see section 4).

Dynamical subapproximations

The major objective of the present study is to examine the baroclinic evolution of meridionally flowing source-driven grounded abyssal currents. However, much (but not all) of the previous work on this subject has examined the problem using a reduced gravity approximation. It is therefore important to show how, in the reduced gravity limit, the model examined here recovers previously described balances. These subbalances are very important in properly interpreting the results of the numerical simulation to be described in Part II (Swaters 2006).

In the inviscid and dynamically uncoupled, or reduced gravity, limit, the abyssal equation in (2.3) reduces to

$$h_t + \frac{h_B' h_y}{1 + \tilde{\beta} y} - \frac{\tilde{\beta} h (h_B' + h_x)}{(1 + \tilde{\beta} y)^2} = Q, \tag{3.2}$$

where it has been assumed, for convenience, that $\tilde{\beta} \equiv s\beta$, $h_B = h_B(x)$, and $h_B' = dh_B(x)/dx$, that is, the topography varies only zonally. As is well known, the reduced gravity limit corresponds, formally, to assuming that the overlying ocean (layers 1 and 2) are infinitely deep and motionless so that the upper layers dynamic pressures are identically zero, that is, the limit $F_1 = F_2 = \phi_1 = \phi_2 = 0$ in (2.1), (2.2), and (2.3). Although it is straightforward to explicitly solve (3.2) using the method of characteristics, the highly implicit form of the solution suggests that it is more valuable to highlight various important subapproximations and to describe these in terms of the existing literature.

1) STOMMEL–ARONS BALANCE

The first subapproximation of interest is the Stommel–Arons balance (Stommel and Arons 1960; Pedlosky 1996, section 7.3) for abyssal flow with a source, in which topography and time dependence is neglected in (3.2), given by

$$\upsilon h = -\frac{(1 + \tilde{\beta} y) Q}{\tilde{\beta}} \Leftrightarrow \beta^* \upsilon^* = -\frac{f Q^*}{h^*}, \tag{3.3}$$

where $\upsilon = h_x/(1 + \tilde{\beta} y)$ [assuming flat topography and no baroclinic coupling; see (2.18)]. Thus, for a source $Q > 0$, there is an equatorward (in either hemisphere) abyssal mass transport induced by the β effect.

2) NOF BALANCE

The next subapproximation of interest is the Nof balance (Nof 1983) for abyssal flow with a source, in which the β effect is neglected in (3.2), given by

$$h_t + h_B'(x) h_y = Q(x, y). \tag{3.4}$$

In fact, in the homogeneous and constant slope limit, (3.4) should be considered only a parsimonious reflection (because the result here assumes a geostrophic balance) of the full Nof (1983) result that showed, for the fully nonlinear reduced gravity shallow water equations, that any isolated (i.e., compactly supported or, equivalently, fully grounded) steadily traveling abyssal water mass, moves with the Nof velocity $(c_x, c_y) = (0, -h_B')$ (or, dimensionally, $c_{y^*}^* = -g' h_B'/f_0$; the x and y subscripts indicate components here and it is assumed that h_B' is a constant) irrespective of the particular height and vorticity distribution within the abyssal water mass.

That is, importantly and perhaps even surprisingly, even in the fully nonlinear regime (but dynamically un-

coupled from the overlying ocean), Nof showed that a grounded abyssal water mass travels nondispersively in the along-slope direction. The Nof (1983) balance provides a dynamical process that can sustain the coherent equatorward movement of grounded deep western abyssal water masses along a continental slope even when far removed from a source region where, presumably, the Stommel–Arons balance initiates equatorward movement.

The solution to the Cauchy problem for (3.4), with an initial condition given by $h(x, y, 0) = \tilde{h}(x, y)$, can be written in the form

$$h(x, y, t) = \tilde{h}[x, y - h'_B(x)t] - \frac{1}{h'_B(x)} \int_y^{y - h'_B(x)t} Q(x, \xi)\, d\xi. \tag{3.5}$$

The solution is composed of two contributions. The first term on the right-hand side of (3.5) is simply the along-slope (geostrophically balanced) motion of the initial abyssal water mass distribution and the second term is the source/sink-created contribution. When $h'_B(x) < 0$ (as occurs, on average, on the western side of a basin), the motion always equatorward (in either hemisphere) since $y - h'_B(x)t \Leftrightarrow (y^* - g' h'_B t^*/f_0)/L$.

Suppose that Q is nonzero only in a localized region, which will be called the source region. In the large time limit, after the transients have propagated away, the Nof balance will be approximately steady near the source region, and governed by

$$uh'_B = -Q \Leftrightarrow u^* = -\frac{Q^*}{(h^*_B)'}, \tag{3.6}$$

where $u = -h_y$ [assuming $h_B = h_B(x)$, $\tilde{\beta} = 0$, and no baroclinic coupling; see (2.18)]. Thus, in a source region $Q > 0$, there is an eastward (in either hemisphere) abyssal mass transport when $h'_B(x) < 0$. Indeed, this is really a Stommel–Arons-like Sverdrup vorticity balance [see (3.3)] for source-driven abyssal flow in which sloping topography replaces the planetary vorticity gradient.

3) Planetary shock wave balance

A third subapproximation of interest is the planetary shock wave balance for abyssal flow with a source (Anderson and Killworth 1979; Johnson and Willmott 1981; Dewar 1987a; Wright and Willmott 1992; Willmott et al. 1996), in which topography is neglected in (3.2), given by

$$h_t - \frac{\tilde{\beta} h h_x}{(1 + \tilde{\beta} y)^2} = Q(x, y). \tag{3.7}$$

The steady-state limit of the planetary shock wave balance (3.7) is the Stommel–Arons Eq. (3.4). Here, again, it is important to emphasize that (3.7) is applicable to grounded abyssal flow. Unfortunately, the name associated with this balance obscures its importance for meridionally flowing abyssal currents. Rather than invent new jargon, the existing terminology is retained.

The solution to (3.7) corresponds to westward propagating (in either hemisphere) abyssal anomalies in which the speed of propagation is proportional to h itself. Thus, as time proceeds, the height profile will tend to steepen on the western side and it is possible for a shock to form, that is, it is possible that $|h_x| \to \infty$ in finite time at a discrete location(s). Wright and Willmott (1992) and Willmott et al. (1996) have analytically and numerically solved (3.7) with steady and periodic Q in a periodic zonal channel.

For example, in the absence of any sources (i.e., $Q = 0$), the solution to the Cauchy problem for (3.7), with initial condition given by $h(x, y, 0) = \tilde{h}(x, y)$, can be written in the form

$$h(x, y, t) = \tilde{h}[\tau(x, y, t), y] \quad \text{and} \quad \tau = x + t\tilde{\beta}\tilde{h}(\tau, y), \tag{3.8}$$

and a shock will first occur the first time $|h_x| \to \infty$, which is given by

$$t_{\text{shock}} = \min_{\tau, y} \left[\frac{1}{\tilde{\beta}\tilde{h}_\tau(\tau, y)} \,|\, \tilde{h}_\tau(\tau, y) > 0 \right]. \tag{3.9}$$

If $(\tau_{\min}, y_{\min})$ is the minimizer associated with (3.9), then the x coordinate of the shock, given by x_{shock}, is determined from

$$\tau_{\min} = x_{\text{shock}} + t_{\text{shock}} \tilde{\beta} \tilde{h}(\tau_{\min}, y_{\min}).$$

Dewar (1987a) has fully explored a number of dynamical properties, and given an oceanographically relevant description of the development and subsequent evolution, of the shocks. Here, it is sufficient to simply remark that the formation of these shocks will correspond to the height or isopycnal field on the upslope or western flank of the abyssal current steepening asymmetrically as compared with the height field on the downslope or eastern flank, as the abyssal water mass flows equatorward.

In addition, the β-induced westward drift associated with (3.7) will tend to counteract the downslope (eastward) motion of perturbation plumes that form on the downslope side of the abyssal current during baroclinic destabilization (Swaters 1991, 1998). That is, the planetary shock wave balance helps to maintain westward intensification and inhibits deep ocean mixing of these equatorward flowing abyssal currents. A more systematic examination of the stability properties is given in section 4.

4) STOMMEL–ARONS–NOF BALANCE

Of particular interest is the structure of the solutions to (3.2) in the full time independent limit, given by

$$\frac{(1+\tilde{\beta}y)}{\tilde{\beta}}h_y - \frac{h}{h'_B}h_x = h + \frac{(1+\tilde{\beta}y)^2 Q(x,y)}{\tilde{\beta}h'_B}. \tag{3.10}$$

This balance can be identified as a combined approximation that includes both Stommel–Arons source-driven flow and steady or long-time Nof flow over sloping topography, which is valid for grounded abyssal currents on a midlatitude β plane. Apparently, this limit has not been examined previously in the literature.

Equation (3.10) can be solved using the method of characteristics. The northeast to southwest orientation of the abyssal flow when $h'_B < 0$ (as occurs, on average, on the western side of a basin) is easily seen from the equation defining the characteristics, given by

$$\left.\frac{dy}{dx}\right|_{\text{characteristic curves}} = -\frac{(1+\tilde{\beta}y)h'_B}{\tilde{\beta}h} > 0.$$

From the point of view of constructing solutions to (3.10) for meridional flow, it is convenient to think of y and x as the timelike and spacelike variables, respectively. The predominate spatial structure of the steady flow predicted by (3.10) can be seen from the unforced problem in which $Q = 0$ and $h = h_0(x)$ along $y = y_0$ is assumed. In this limit, the solution is given by

$$h(x,y) = h_0[\tau(x,y)](1+\tilde{\beta}y)/(1+\tilde{\beta}y_0) \quad \text{and}$$
$$h_B(x) = h_B(\tau) + \tilde{\beta}h_0(\tau)(y_0 - y)/(1+\tilde{\beta}y_0). \tag{3.11}$$

In section 4, a variational principle is established for solutions of the form (3.11) in the context of the baroclinic problem and this principle is used to derive general linear baroclinic stability conditions. In addition, the spatial and temporal baroclinic instability characteristics are described for a specific solution.

It follows from (3.11) that there is a linear thinning of the thickness of the abyssal layer as y decreases (i.e., in the equatorward direction) along the characteristic curves. This follows because the potential vorticity for the abyssal layer, given by $(1+\tilde{\beta}y)/h$ in the reduced-gravity PG approximation, is invariant following the steady abyssal flow. Since the Coriolis parameter decreases linearly in the equatorward direction on a midlatitude β plane, so too, must the abyssal layer height.

Although it may not seem immediately apparent, (2.3) and hence (3.2) and (3.10), is the potential vorticity equation for the abyssal layer. To see this, (2.3) is first rewritten [see, also, (A.9)], in the reduced gravity limit, in the (usual mass equation) form

$$h_t + \nabla\cdot[\mathbf{e}_3 \times \nabla(h_B + h)h/(1+\tilde{\beta}y)] = Q + r_3\Delta(h_B + h),$$

which, when multiplied through by $-(1+\tilde{\beta}y)/h^2$, can be rewritten as

$$\left(\frac{f}{h}\right)_t + \mathbf{u}\cdot\nabla\left(\frac{f}{h}\right) = -f[Q + r_3\Delta(h_B + h)]/h^2, \tag{3.12}$$

where $f \equiv 1 + \tilde{\beta}y$ and $\mathbf{u} = \mathbf{e}_3 \times \nabla\,(h_B + h)/f$. Thus, if $Q = r_3 = 0$, then f/h is conserved following the motion [which, in addition to time independence, are the assumptions upon which the solution (3.11) has been derived].

In the notation of (3.12), (3.10) can be rewritten in the form

$$\mathbf{u}\cdot\nabla\left(\frac{f}{h}\right) = -fQ/h^2. \tag{3.13}$$

The relative simplicity of (3.13) masks the fact that it models, within the most simple assumptions, equatorward source-driven grounded abyssal flow as process initiated as Stommel–Arons source-driven abyssal flow that transitions to an inertial Nof balance abyssal flow. The role of $\tilde{\beta}$ is to inhibit baroclinic instability and helps to maintain westward intensification. This is further discussed in section 4.

It is possible that $|h_x| \to \infty$ at a particular (x, y) location for the solution (3.11). Assuming $h'_B < 0$, these "shocks" will first occur on the upslope side of the abyssal current at the y value given by

$$y_{\text{shock}} = y_0 - \min_{\tau}\left[-\frac{h'_B(\tau)(1+\tilde{\beta}y_0)}{\tilde{\beta}h'_0(\tau)}\,|h'_0(\tau) > 0\right] \le y_0. \tag{3.14}$$

If this situation arises, the solution will no longer be valid in the region $y < y_{\text{shock}}$. However, this is not a physically relevant result since there are, in the full model, many other physical processes occurring to prevent this mathematical singularity from developing. If $\tau_{\min}$ is the minimizer associated with (3.14), then the x coordinate of the shock, given by x_{shock}, is determined from

$$h_B(x_{\text{shock}}) = h_B(\tau_{\min}) + \tilde{\beta}h_0(\tau_{\min})(y_0 - y_{\text{shock}})/(1+\tilde{\beta}y_0).$$

To provide a specific illustration of the meridional structure associated with the Stommel–Arons–Nof inertial solution (3.11), consider the example where $h_B = -x - 12$ (the constant -12 has been added for graphical convenience only, see Fig. 2b) and

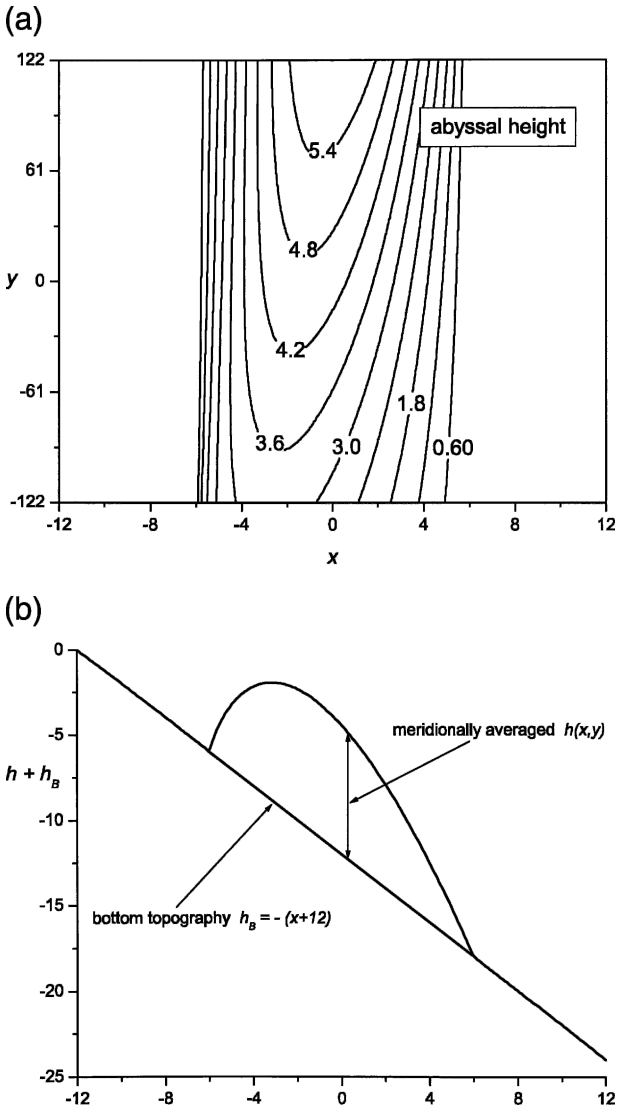

FIG. 2. (a) Contour plot of $h(x, y)$ as determined by (3.11) and (3.15). The contour interval is 0.6. (b) The meridionally averaged total abyssal height $h(x, y) + h_B(x)$, as determined by (3.11) and (3.15) with $h_B(x) = -x - 12$. A nondimensional height of 1.0 corresponds to about 84 m.

$$h_0(x) = \begin{cases} \tilde{h}[1 - (x/a)^2], & \text{for} \quad -a \le x \le a, \\ 0, & \text{otherwise}, \end{cases} \tag{3.15}$$

along $y = y_0$, which corresponds to an along-slope abyssal flow that is transversely grounded in both the up- and downslope directions, that is, $h_0(\pm a) = 0$ with maximum (nondimensional) height given by $\tilde{h}$ located at $x = 0$ (similar to that depicted in Fig. 1). Note that since both the abyssal layer height and the bottom topography have been scaled using the bottom slope [see (2.7d)], it is appropriate to introduce a free height parameter for (i.e., $\tilde{h}$) and set the absolute value of the constant bottom slope to be 1.0.

The choice of a linearly sloping bottom is motivated by the fact that the equations can be solved exactly (although the solution does not have a simple height field and does not correspond to a parallel shear flow). Ideally, the topographic profile should vary more or less linearly with respect to the zonal coordinate near a coast and then transition to a flat bottom in the mid-ocean. In Part II (Swaters 2006), which presents the numerical simulation, zonally varying topography that is derived from North Atlantic bathymetry is introduced, which has exactly this property. The goal in this subsection is to identify the salient dynamical characteristics of the model in as simple a configuration as possible in order to provide guideposts for the substantially more complex solution contained in Part II.

Substitution of (3.15) into the second equation of (3.11) implies

$$\tau(x, y) = \frac{2\left[x + \dfrac{\tilde{\beta}\tilde{h}(y_0 - y)}{(1 + \beta y_0)}\right]}{1 + \sqrt{1 + \dfrac{4\tilde{\beta}\tilde{h}(y_0 - y)}{a^2(1 + \tilde{\beta}y_0)}\left[x + \dfrac{\tilde{\beta}\tilde{h}(y_0 - y)}{(1 + \tilde{\beta}y_0)}\right]}}, \tag{3.16}$$

when $-a \le \tau \le a$. If $|\tau| > a$, then $h(x, y) = 0$, and note that $\tau(x, y_0) = x$. It follows from (3.14) that

$$y_{\text{shock}} = y_0 - \frac{a(1 + \tilde{\beta}y_0)}{2\tilde{\beta}\tilde{h}}. \tag{3.17}$$

For this example, the initial abyssal meridional transport through the section $y = y_0$, denoted by $\mathcal{T}_0$, is given by

$$\mathcal{T}_0 = \int_{-a}^{a} (vh)_{y=y_0}\, dx = \int_{-a}^{a} \frac{(h_0 + h_B)_x h_0}{(1 + \tilde{\beta}y_0)}\, dx$$
$$= -\frac{4\tilde{h}a}{3(1 + \tilde{\beta}y_0)}.$$

Further discussion of the solution is facilitated by selecting specific values for the parameters. Suppose $a = \tilde{h} = 6$ and $y_0 = 122$ is chosen. Based on the scalings in section 2, these values imply that $h_0(x)$ corresponds to a grounded parabolically shaped abyssal current located at 60°N with maximum height or thickness of 500 m and width of 180 km with a southward transport of about $\mathcal{T}_0 \simeq 37.13$ that, dimensionally, is about 1.4 Sv (Sv $\equiv 10^6$ m^3 s^{-1}).

It follows from (3.17) that a shock will form at $y_0 - y_{\text{shock}} \simeq 269.33$, which is equivalent to a location 4040 km southward of the latitude of initialization. The large distances from the point of flow initialization associated with the shock formation almost certainly implies that in the real ocean, with its vast array of additional physics, this singularity never actually develops.

In Fig. 2a, a contour plot of the nondimensional height $h(x, y)$, as determined by (3.11) and (3.15) with the above parameter values is shown. The contour interval is 0.6 and a nondimensional height of 1.0 corresponds to 84 m. The meridional extent of the domain is given by $-122 < y < 122$ (about 40° of latitude, or 3660 km centered at 40°N) and, for convenience, the zonal extent is restricted to the region $-12 < x < 12$.

Two properties are seen in Fig. 2a. First, there is a gradual decrease in the maximum height of the abyssal current in the equatorward direction. This occurs because the flow is conserving PG potential vorticity [recall $Q = 0$ in this example; see (3.13)]. Second, there is a westward displacement of the point of maximum height as the current flows southward. This is also due to $\tilde{\beta}$ and is the result of the planetary shock wave–like balance in (3.10) where time dependence has been replaced by the gradient associated a sloping bottom [cf. (3.7) and (3.10)].

Figure 2b is a plot of the along-slope or meridionally averaged total abyssal height $h(x, y) + h_B(x)$, given by

$$h_B(x) + \frac{1}{244}\int_{-122}^{122} h(x, y)\, dy,$$

where $h(x, y)$ is determined by (3.11) and (3.15). Thus, notwithstanding the westward displacement just described, in an averaged sense, the parabolically shaped cross-slope structure of the initial abyssal current is maintained meridionally with clearly defined up- and downslope groundings (like those idealized in Fig. 1). These features are characteristic of the deep western boundary undercurrent in the North Atlantic (see e.g., Richardson 1977).

The northward velocity is given by $v = (h + h_B)_x/(1 + \tilde{\beta}y)$, so that the cross-slope-averaged v associated with Fig. 2b would be given by

$$\frac{1}{244}\int_{-122}^{122}\left(\int_{-12}^{12}\chi_h v\, dx/\int_{-12}^{12}\chi_h\, dx\right) dy =$$

$$-\frac{1}{244\tilde{\beta}}\ln\left(\frac{1 + 122\tilde{\beta}}{1 - 122\tilde{\beta}}\right) \simeq -1.03,$$

where χ_h is the characteristic function for h; that is, $\chi_h = 1$ if $h > 0$ and $\chi_h = 0$ if $h = 0$ [$\tilde{\beta} = 0.0024$ has been used; see (2.5)]. Because the scaling for the abyssal velocity field is the Nof speed [see the discussion following (2.5)], it follows that the abyssal current depicted in Fig. 2b flows out of the page with an average speed of about 3 cm s^{-1}. This is consistent with observations of the deep western boundary undercurrent in the North Atlantic (see, e.g., Richardson 1977).

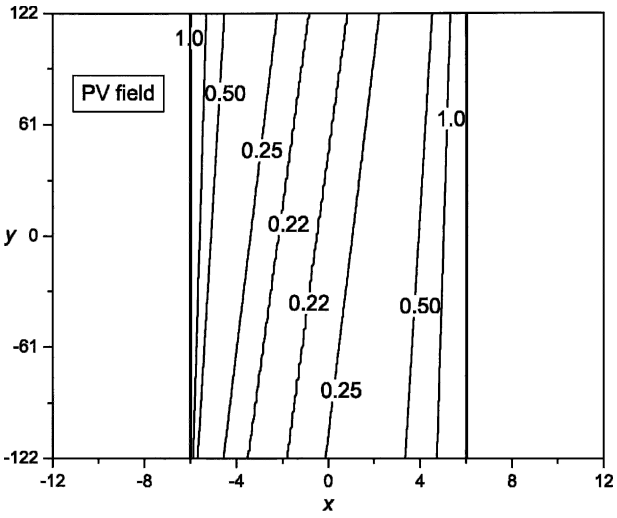

FIG. 3. Contour plot of the potential vorticity field $(1 + \tilde{\beta}y)/h(x, y)$, as determined by (3.11) and (3.15), for selected contours. The abyssal current pathlines are parallel to the isolines of potential vorticity.

Since the solution is unforced, (3.13) implies that the potential vorticity is constant along the pathlines (there is no streamfunction for the velocity field). That is, the Lagrangian trajectories are along the isolines of the PG potential vorticity. In Fig. 3a contour plot of the PG potential vorticity $(1 + \tilde{\beta}y)/h$ is shown. Because, in the PG approximation, the potential vorticity becomes infinite on the zero-height contour, potential vorticity values greater than 1.0 in value are not shown. Although it cannot be inferred from Fig. 3, the flow is generally oriented in the northeast to southwest direction.

In Fig. 4a the zonally averaged abyssal height $\langle h\rangle$, defined by

$$\langle h\rangle(y) = \int_{-12}^{12} h(x, y)\, dx/\int_{-12}^{12}\chi_h\, dx, \qquad (3.18)$$

is shown. The linear decrease in $\langle h\rangle$, associated with potential vorticity conservation as y decreases, is clear.

In Fig. 4b the meridional transport, denoted by $\mathcal{T}(y)$, and given by

$$\mathcal{T}(y) = \int_{-12}^{12} vh\, dx = \int_{-12}^{12}\frac{(h + h_B)_x h}{(1 + \tilde{\beta}y)}\, dx$$

$$= -\int_{-12}^{12}\frac{h}{(1 + \tilde{\beta}y)}\, dx, \qquad (3.19)$$

is shown. The linear decrease in h as the current flows equatorward is, of course, in this adiabatic solution, exactly offset by the linearly decreasing Coriolis parameter in the denominator of (3.19) (i.e., the equatorward abyssal speed increases in the equatorward direction)

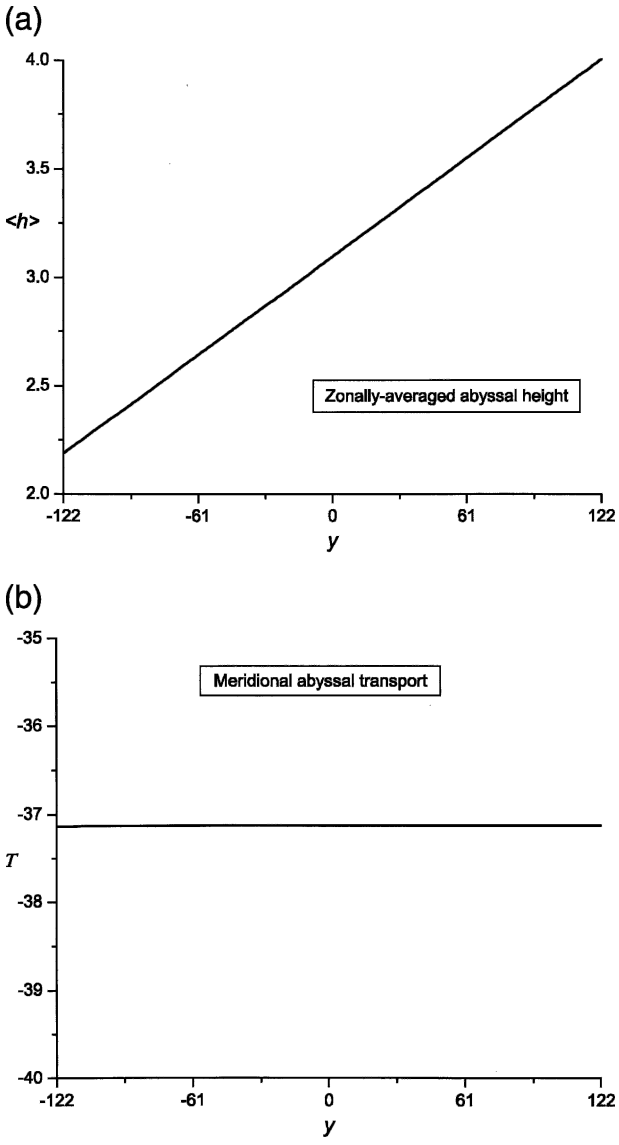

FIG. 4. (a) The zonally averaged abyssal height $\langle h \rangle$ vs y for the solution determined by (3.11) and (3.15). The linear decrease in $\langle h \rangle$ as y decreases is a consequence of PG PV conservation. Dimensionally, $\langle h \rangle = 1$ corresponds to about 84 m. (b) The meridional abyssal transport $\mathcal{T}$ vs y for the solution determined by (3.11) and (3.15). The transport is constant as a consequence of the fact that the linear decrease in h is canceled by the decrease in the Coriolis parameter in the denominator of (3.19) as the flow moves southward. Dimensionally, $\mathcal{T} = 1$ corresponds to about 3.8×10^{-2} Sv.

to yield a constant transport of about $\mathcal{T}(y) \simeq 37.13$ that, dimensionally, is equivalent to about 1.4 Sv.

4. Baroclinic instability characteristics

The general theoretical baroclinic instability characteristics for inertial grounded abyssal flow over sloping topography on an f plane, in the two-layer and continuously stratified versions of the model, have been described by Swaters (1991, 1993, 1998), Mooney and Swaters (1996), Poulin and Swaters (1999), Reszka et al. (2002), Pavec et al. (2005), and Ha and Swaters (2006). Karsten et al. (1995) and Choboter and Swaters (2000) used the two-layer f-plane model to describe the stability characteristics of deep water replacement in the Strait of Georgia and rotating tank experiments, respectively. Reszka et al. (2002) used a continuously stratified version of the f-plane model to describe the stability characteristics of the Denmark Strait Overflow. The purpose of this section is to describe the linear instability characteristics when β is present.

In summary, the instability mechanism is the release of the available gravitational potential energy associated with grounded dense water sitting directly on a sloping bottom surrounded by relatively lighter water. As the center of mass of the perturbed grounded abyssal water mass slides down the sloping bottom, its gravitational potential energy is released as perturbation kinetic energy in the overlying ocean, through the action of vortex stretching. That is, associated with the destabilization, cold dense abyssal water moves in the downslope direction, while warm lighter overlying water moves in the up slope direction. Since the sloping bottom is a topographic β plane for the upper QG layer(s) [see (2.2)], this is exactly identical to the process of midlatitude baroclinic instability for zonal flow, in which available potential energy is released as warm equatorial fluid moves poleward and a cold polar fluid moves equatorward. From a modal point of view, the instability is a consequence of the coalescence of two topographic vorticity waves that have been excited in the overlying water column.

For an unstable abyssal current that has a transverse thickness profile shaped parabolically like a coupled front [such as (3.15); see Figs. 1 and 2b], the instability theory predicts that the perturbations in the abyssal layer take the form of along-slope traveling waves that preferentially amplify on the downslope side of the abyssal current, which subsequently develop into downslope propagating plumes. The downslope perturbation plumes do not, however, continue to move into the deeper ocean unabated. In the nonlinear regime, the downslope plumes geostrophically adjust and can develop into coherent abyssal domes that propagate in the along-slope direction. The amplifying perturbations on the upslope and downslope groundings are asymmetric (i.e., neither sinuous nor varicose in structure) in contrast to that predicted by barotropic (i.e., horizontal shear based) instability theory (see Fig. 9 in Swaters 1991; Fig. 7 in Karsten et al. 1995; Plate 1 in Swaters 1998; or Figs. 7 and 13 in Reszka et al. 2002). This

asymmetry is a unique signature of the baroclinic destabilization of these grounded abyssal currents.

To examine the baroclinic instability problem in its simplest form, but still retaining the most important features, the inviscid, stress-free, rigid-lid, and 2½-layer approximation

$$F_{1,2} = \phi_1 = \Upsilon = r_{2,3} = 0, R_e \to \infty,$$

is introduced into (2.1), (2.2), and (2.3), yielding

$$(\Delta\eta + h)_t + J(\eta, \Delta\eta + h + h_B + \beta y) = 0 \quad (4.1)$$

and

$$h_t + J\left(h + \eta + h_B, \frac{h}{1 + s\beta y}\right) = Q, \quad (4.2)$$

where, for convenience, $\eta \equiv \phi_2$. The reason that there is no up/downwelling Q term in (4.1) is because the upper QG layer (i.e., layer 1) is assumed infinitely deep and quiescent. Equations (4.1) and (4.2) are the same as the Swaters (1991) model with β and Q included.

The area integrated energy for (4.1) and (4.2) is given by

$$\mathcal{E}(\eta, h) = \frac{1}{2}\iint_\Omega \boldsymbol{\nabla}\eta \cdot \boldsymbol{\nabla}\eta + (h + h_B)^2 - h_B^2 \, dx\, dy, \quad (4.3)$$

which will be invariant, that is, $d\mathcal{E}/dt = 0$, in the inertial limit $Q = 0$. If $Q = 0$, (4.1) and (4.2) is a 2×2 infinite dimensional Hamiltonian dynamical system (see, e.g., Swaters 1993, 2000), in which $\mathcal{E}$ will be the Hamiltonian functional and the Hamiltonian variables are given by $\Delta\eta + h$ and h, respectively. The Casimirs (i.e., the set of invariant functionals that span the Kernel of the Poisson bracket; see Swaters 2000), which are needed in the variational principle, may be written in the form

$$C_1 = \iint_\Omega \left[\int_{h_B+\beta y}^{\Delta\eta+h+h_B+\beta y} \mathcal{F}_1(\xi)\, d\xi\right] dx\, dy \quad (4.4)$$

and

$$C_2 = \iint_\Omega (1 + s\beta y)\left[\int_0^{h/(1+s\beta y)} \mathcal{F}_2(\xi)\, d\xi\right] dx\, dy, \quad (4.5)$$

where $\mathcal{F}_{1,2}$ are arbitrary functions of their arguments.

a. Steady solutions, variational principle, and stability conditions

General inertial steady abyssal solutions to (4.1) and (4.2) of the form

$$\eta = \tilde{\eta} = 0, h = \tilde{h}(x, y), h_B = h_B(x, y), \quad \text{and} \quad Q = 0 \quad (4.6)$$

must satisfy

$$J\left(\tilde{h} + h_B, \frac{\tilde{h}}{1 + s\beta y}\right) = 0, \quad (4.7)$$

which implies that

$$\tilde{h} + h_B = \mathcal{F}\left(\frac{\tilde{h}}{1 + s\beta y}\right), \quad (4.8)$$

for some function $\mathcal{F}$. The reason that $\tilde{\eta} = 0$ has been chosen is to focus attention on the baroclinic destabilization of abyssal currents in the absence of any mean flow in the overlying layer. Sutherland et al. (2004) have described rotating-tank experiments investigating the role of barotropic instability in the upper layer associated with source-driven abyssal currents.

As an example, in the case where $h_B = h_B(x)$, (4.7) is identical to (3.10) (with $Q = 0$) and thus (3.11) solves (4.7). It follows for (3.11) that

$$\mathcal{F}(\xi) = (1 + s\beta y_0)\xi + h_B\{h_0^{-1}[(1 + s\beta y_0)\xi]\}, \quad (4.9)$$

where h_0^{-1} is the inverse function associated with h_0. Although the introduction of the function $\mathcal{F}$ may seem abstract, its use is the most economical way to derive the stability conditions. Note that if $\beta \neq 0$, all steady inertial solutions for $\tilde{h}$ must depend on both x and y and the solution does not correspond to a parallel shear flow.

The solution (4.8) (with $\tilde{\eta} = 0$ understood) satisfies the first-order conditions for an extremal of the invariant functional

$$\begin{aligned} I &\equiv \mathcal{E} + C_1 + C_2 \\ &= \mathcal{E} - \iint_\Omega (1 + s\beta y)\left\{\int_0^{h/(1+s\beta y)} \mathcal{F}(\xi)\, d\xi\right\} dx\, dy, \end{aligned} \quad (4.10)$$

where $\mathcal{F}_1 = 0$ and $\mathcal{F}_2 = -\mathcal{F}$. It follows (assuming $\eta = 0$ on the boundary of Ω) that

$$\begin{aligned} \delta I(\eta, h) &= \iint_\Omega -\eta\Delta\delta\eta + \left[h + h_B - \mathcal{F}\left(\frac{h}{1 + s\beta y}\right)\right]\delta h\, dx\, dy \\ &= \iint_\Omega -\eta(\Delta\delta\eta + \delta h) \\ &\quad + \left[h + \eta + h_B - \mathcal{F}\left(\frac{h}{1 + s\beta y}\right)\right]\delta h\, dx\, dy, \end{aligned} \quad (4.11)$$

so that $\delta I(\tilde{\eta}, \tilde{h}) = 0$.

The second variation of I evaluated at the steady solution $(\tilde{\eta}, \tilde{h})$ is given by

$$\delta^2 I(\tilde{\eta}, \tilde{h}) = \iint_{\Omega} \nabla\delta\eta \cdot \nabla\delta\eta + \left[1 - \frac{\mathcal{F}'\left(\dfrac{\tilde{h}}{1 + s\beta y}\right)}{(1 + s\beta y)}\right](\delta h)^2\, dx\, dy = \iint_{\Omega} \nabla\delta\eta \cdot \nabla\delta\eta - \frac{h_{B_x}(x, y)}{\tilde{h}_x(x, y)}(\delta h)^2\, dx\, dy, \tag{4.12}$$

where the prime means differentiation with respect to the argument and (4.8) has been used. It is always the case that $\delta^2 I(\tilde{\eta}, \tilde{h})$ is an invariant of the linear stability equations [see (4.17) and (4.18)] where the perturbations are $(\delta\eta, \delta h)(x, y, t)$ (Swaters 2000). Since the integrand of the functional $\delta^2 I(\tilde{\eta}, \tilde{h})$ is a diagonalized quadratic form with respect to $(\delta\eta, \delta h)$ if $\delta^2 I(\tilde{\eta}, \tilde{h})$ is definite in sign for all perturbations, then $(\tilde{\eta}, \tilde{h})$ is linearly stable {in the sense of Liapunov with respect to the norm $[|\delta^2 I(\tilde{\eta}, \tilde{h})|]^{1/2}$}.

The case in which $\delta^2 I(\tilde{\eta}, \tilde{h}) < 0$ is not considered. It requires certain mathematical properties to hold on the domain Ω, and while these can occur this analysis is not pursued [see Swaters (1993) for the *f*-plane Hamiltonian-based analysis]. The case in which $\delta^2 I(\tilde{\eta}, \tilde{h}) > 0$ is precisely analogous to Fjørtoft's stability theorem (Swaters 2000) and reduces to the *f*-plane results of Swaters (1991, 1993).

It follows from (4.12) that $\delta^2 I(\tilde{\eta}, \tilde{h}) > 0$ when

$$\frac{h_{B_x}(x, y)}{\tilde{h}_x(x, y)} \leq 0. \tag{4.13}$$

This is a sufficient condition for stability. A necessary condition for instability is, therefore, that there exists at least one point $(x, y) \in \Omega$ for which

$$\frac{h_{B_x}(x, y)}{\tilde{h}_x(x, y)} > 0. \tag{4.14}$$

Even though β has been fully retained, this stability condition is identical in form to that obtained by Swaters (1991).

Consider the case in which $h_{B_x}(x, y) < 0$ as would occur, on average, along the western shelf–slope region of an ocean basin. The necessary condition for instability is that there exists at least one point for which $\tilde{h}_x(x, y) < 0$. For a parabolically shaped abyssal current with upslope and downslope groundings (like that depicted in Figs. 1 and 2b), this condition holds on the downslope flank but not on the upslope flank. This is why the instability preferentially amplifies on the downslope flank and the amplitude of the perturbations along the downslope grounding are much larger relative to those on the upslope grounding (see Swaters 1991, 1998). Physically, energy is required to move grounded abyssal fluid parcels located adjacent to the upslope grounding up the sloping bottom (against the force of gravity), while energy is released by the downslope movement of grounded abyssal fluid parcels located along the downslope grounding. The result is that there is a spatial asymmetry (even on an *f* plane) in the process of destabilization of these grounded abyssal currents. This asymmetry is clearly seen in numerical simulations (e.g., Jiang and Garwood 1996; Swaters 1998) and laboratory experiments (Etling et al. 2000) and has been attributed to the Swaters's instability mechanism (Jungclaus et al. 2001). This is in sharp contrast to the symmetry (i.e., varicose or sinuous) in destabilized surface intensified buoyancy driven currents. This is the reason why results from the laboratory modeling of grounded abyssal currents on a sloping bottom as surface-intensified buoyancy-driven currents do not agree with theory (e.g., Griffiths et al. 1982) as discussed by Swaters (1991) and Karsten et al. (1995).

There are no unforced steady solutions to (4.1) and (4.2) that are independent of *y*. The steady meridional abyssal flow over zonally varying topography given by

$$\eta = 0, h = h_0(x), \quad \text{and} \quad h_B = h_B(x) \tag{4.15}$$

is an exact solution to (4.1) and (4.2) provided

$$Q(x, y) \equiv -s\beta h_0(h_B' + h_0')/(1 + s\beta y)^2. \tag{4.16}$$

If the $s\beta y$ term is neglected in (4.2) [but β is still retained in (4.1)], Q is not required to balance this steady flow.

b. *Baroclinic instability characteristics for a constant abyssal current*

The general linear baroclinic stability equations (valid for either the inertial or forced situations) are obtained by substituting

$$\eta = \hat{\eta}(x, y, t), h = h_0(x, y) + \hat{h}(x, y, t), \quad \text{and} \quad h_B = h_B(x, y)$$

into (4.1) and (4.2) and linearizing, yielding

$$(\Delta\eta + h)_t + J(\eta, h_0 + h_B + \beta y) = 0 \tag{4.17}$$

and

$$h_t + J\left(h + \eta, \frac{h_0}{1 + s\beta y}\right) + J\left(h_0 + h_B, \frac{h}{1 + s\beta y}\right) = 0, \tag{4.18}$$

where the caret has been dropped, and it is assumed that

$$Q \equiv J\left(h_0 + h_B, \frac{h_0}{1 + s\beta y}\right). \tag{4.19}$$

The forcing $Q = 0$ if (4.7) holds (i.e., the abyssal flow is an inertial solution in the reduced gravity approximation), otherwise, in general, it is nonzero, for example, for a parallel shear flow of the form (4.15).

The linear stability problem is, as written, analytically intractable. However, much can be learned from the constant-velocity abyssal flow on the linearly sloping bottom, given by

$$h_0 = \tilde{h} - \gamma x \geq 0, \quad \text{and} \quad h_B = -x, \tag{4.20}$$

where $\tilde{h} > 0$ is constant, and neglecting terms of $O(s\beta)$ in (4.18) but retaining β in (4.17). The abyssal height (4.20) is the simplest profile for h_0 that satisfies the necessary condition for instability (4.14) and for which the stability problem can be solved explicitly. It is noted that the linear stability equations can be solved exactly for a quadratically shaped abyssal height profile [e.g., such as (3.15)] with groundings, by extending the solution procedure developed by Swaters (1991). However, the most important stability characteristics can be described using the simple constant flow (4.20) (in much the same way as the Phillips model reveals important properties of baroclinic instability on the β plane).

In Part II (Swaters 2006), a numerical simulation will be described with $Q \neq 0$ (the support of Q is restricted to a localized region in the northwest corner of the domain), and with zonally varying topography (as derived from North Atlantic bathymetry) that varies linearly near the western side of the basin and transitions to a flat bottom in the midocean. The source-driven meridionally flowing abyssal current that is produced will possess both up- and downslope groundings. Again, the goal in this subsection is to identify the most important baroclinic instability characteristics of the model in as simple a configuration as possible in order to provide guideposts for the substantially more complex solution contained in Part II.

Neglecting terms of $O(s\beta)$ in (4.18) is physically reasonable in the context of the baroclinic instability problem since $s\beta \simeq 10^{-3}$ [see (2.5)] and the most unstable modes will, it can be expected, have along-slope wavelengths on the order of the internal deformation radius, which is the horizontal length scale; that is, the wavelengths will be $O(1)$ as shown below. This approximation implies that $\eta = 0$ and $h = h_0(x)$ is a nonlinear inertial steady solution to (4.1) and (4.2) (i.e., $Q = 0$) so that the stability theory developed in section 4a is applicable. In this limit, the steady abyssal velocity is given by $\mathbf{u}_{\text{abyssal0}} = -(0, 1 + \gamma)$ and the necessary condition for instability is $\gamma > 0$.

Substitution of (4.20) into (4.17) and (4.18) implies that the linear stability equations can be written in the form

$$\Delta\eta_t + \beta\eta_x + (h + \eta)_y = 0 \quad \text{and} \quad h_t - h_y + \gamma\eta_y = 0. \tag{4.21}$$

These equations will be solved in the meridional channel domain $x \in (0, L)$ so that the appropriate boundary condition is $\eta = 0$ on $x = 0, L$. It is convenient to write the normal mode solution using the "carrier-wave transformation" (Longuet-Higgins 1965), in the form

$$(h, \eta) = A[\gamma/(1 + c), 1] \sin(n\pi x/L) \exp[ik(y - ct) - i\beta x/(2ck)] + \text{c.c.}, \tag{4.22}$$

where $n \in \mathbb{Z}^+$, c.c. means the complex conjugate of the preceding term, k is the meridional, or along-slope, wavenumber, A is a free-amplitude constant, and c is the complex-valued phase velocity that must satisfy the dispersion relationship

$$K^2c^3 + (1 + K^2)c^2 + \left[1 + \gamma - \left(\frac{\beta}{2k}\right)^2\right]c - \left(\frac{\beta}{2k}\right)^2 = 0, \tag{4.23}$$

where $K \equiv \sqrt{k^2 + l^2}$ is the wavenumber modulus and $l \equiv n\pi/L$.

The three roots to the cubic dispersion relation (4.23) correspond to a barotropic and baroclinic topographic Rossby wave and to a planetary Rossby wave, respectively. The onset of instability corresponds to the coalescence of the barotropic and baroclinic topographic Rossby modes. Mathematically, this coalescence occurs when the discriminate for the cubic is zero and this condition defines the marginal stability boundary. Thus, the marginal stability boundary is given by

$$\varsigma_1^3 - \left(\frac{\varsigma_2\varsigma_1}{2}\right)^2 - \frac{9\varsigma_1\varsigma_2\varsigma_3}{2} + \frac{27\varsigma_3^2}{4} + \varsigma_2^3\varsigma_3 = 0, \tag{4.24}$$

where

$$\varsigma_1 \equiv \frac{1 + \gamma - \left(\frac{\beta}{2k}\right)^2}{K^2}, \; \varsigma_2 \equiv 1 + K^{-2}, \quad \text{and} \quad \varsigma_3 \equiv -\left(\frac{\beta}{2kK}\right)^2. \tag{4.25}$$

Equation (4.24) is itself a cubic with respect to ς_1 (i.e., γ). It can be shown that the discriminate for (4.24) is

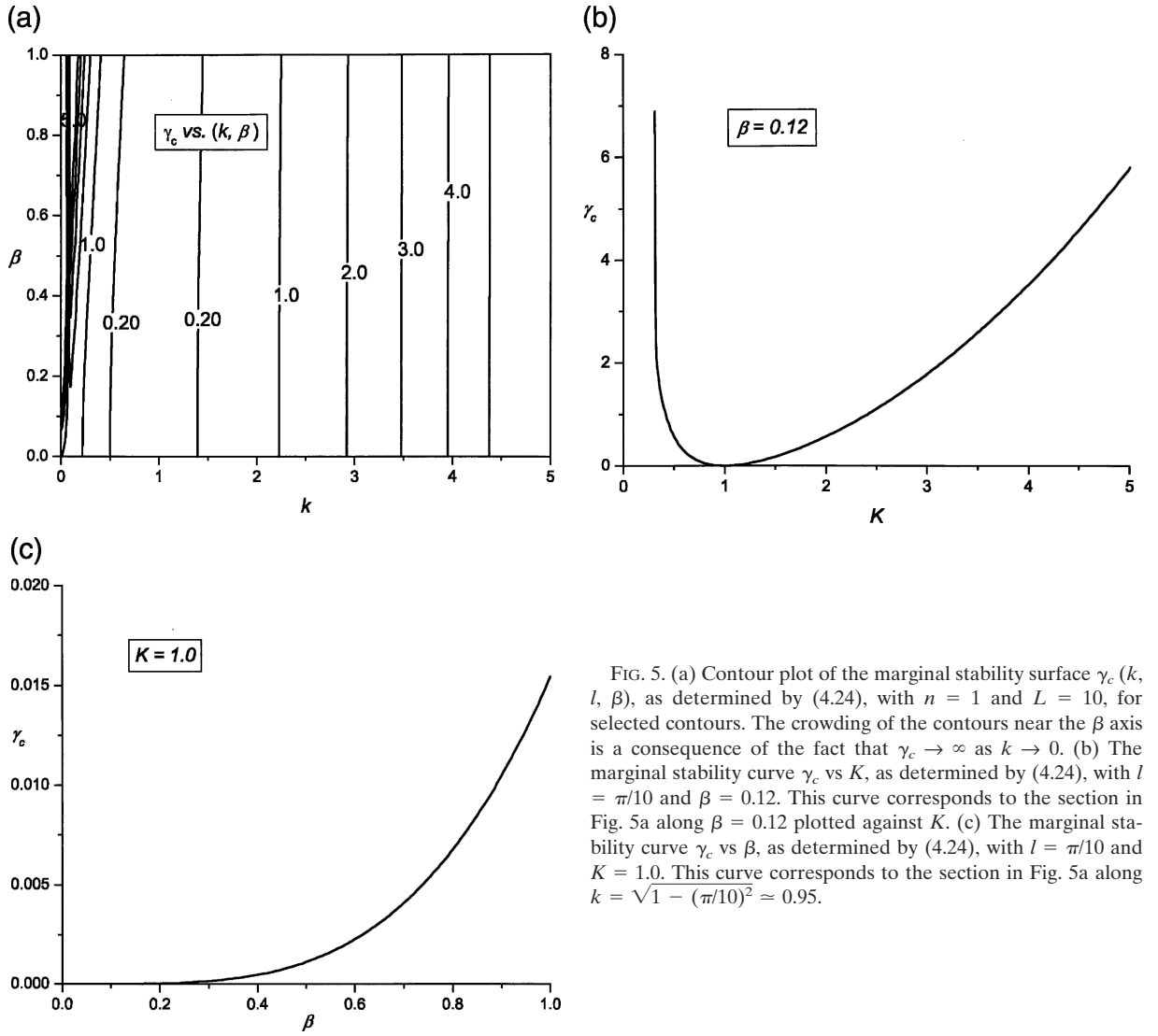

FIG. 5. (a) Contour plot of the marginal stability surface γ_c (k, l, β), as determined by (4.24), with $n = 1$ and $L = 10$, for selected contours. The crowding of the contours near the β axis is a consequence of the fact that $\gamma_c \to \infty$ as $k \to 0$. (b) The marginal stability curve γ_c vs K, as determined by (4.24), with $l = \pi/10$ and $\beta = 0.12$. This curve corresponds to the section in Fig. 5a along $\beta = 0.12$ plotted against K. (c) The marginal stability curve γ_c vs β, as determined by (4.24), with $l = \pi/10$ and $K = 1.0$. This curve corresponds to the section in Fig. 5a along $k = \sqrt{1 - (\pi/10)^2} \simeq 0.95$.

strictly positive since $\varsigma_2 > 0$ and $\varsigma_3 < 0$ ($\beta > 0$) and is zero only if $\beta = 0$. Thus, there is only one real solution for γ, denoted as $\gamma_c(k, l, \beta)$, and this is the marginal stability boundary (or, equivalently, the critical abyssal slope or equatorward velocity). That is, for a given k, l, and β, instability only occurs if $\gamma > \gamma_c$, (neutral) stability occurs if $\gamma \leq \gamma_c$ and the marginal stability boundary is given by $\gamma = \gamma_c(k, l, \beta)$. The point of marginal stability will be the minimum $\gamma_c \geq 0$, with respect to k and l, for fixed β. In the limit $\beta = 0$, (4.24) reduces to $\gamma_c = (K^2 - 1)^2/(4K^2)$, which is the f-plane result of Mooney and Swaters (1996).

Figure 5a shows a contour plot of γ_c in the (k, β) plane for the gravest cross channel mode $n = 1$ with a cross-channel width of 10 (deformation radii); that is, $l = \pi/10$. The marginal stability is concave up with respect to k with a modest, but positive monotonic, dependence on β. It is seen that γ_c increases monotonically as $k \to 0$ or ∞ (actually $\gamma_c \to \infty$ as $K \to 0$ or ∞) irrespective of β with the minimum γ_c (the point of marginal stability) located near $K = 1$.

Figure 5b shows a section from Fig. 5a for γ_c versus K along $\beta = 0.12$ (that is a characteristics value for β based on the scalings introduced section 2). The abscissa has been chosen as K to facilitate comparison with the f-plane marginal stability curve shown in Fig. 2 from Mooney and Swaters (1996). The point of marginal stability is located at $\gamma = 0$ and $K \simeq 1.0$ (K is actually very slightly larger than 1.0).

Figure 5b is to be compared, for example, with the marginal stability curve for the baroclinic instability of a zonal flow on a β plane in the Phillips model (see Fig. 7.11.1a in Pedlosky 1987). The principal difference is that in the Phillips model, instability only occurs for a

finite band of wavenumbers irrespective of the critical shear (i.e., γ), which results in the marginal stability curve becoming unbounded at a finite nonzero wavenumber, whereas in the abyssal model considered here, the high wavenumber cutoff is an increasing function of the shear (see Mooney and Swaters 1996) so that γ_c exists for all nonzero K. This difference is a consequence of the fact that the PG approximation in the abyssal layer is equivalent to an infinite deformation assumption (within the abyssal layer only), which leads to the abyssal rotational Froude number being zero.

Figure 5c shows a section from Fig. 5a for γ_c versus β along $K = 1.0$ (the wavenumber of the marginally unstable mode for $\beta = 0$). The gradual monotonic increase in γ_c as β increases is clearly seen. This illustrates the (slightly) stabilizing influence of β.

The coalescence of the topographic wave modes for the instability to occur is seen in Figs. 6a,b. In Figs. 6a,b the frequencies [$\omega = k\mathrm{Re}(c)$] and growth rates [$\sigma = k\mathrm{Im}(c)$], respectively, versus k for the three solutions for c as determined by (4.23), for the parameter values $\beta = 0.12$, $\gamma = 1.0$, and $l = \pi/10$, is shown. As follows from Fig. 5b, there is only a finite interval of wavenumbers that are unstable for these parameter values (i.e., there is a low and high wavenumber cutoff; see, also, Mooney and Swaters 1996). Accordingly, in Fig. 6a, there are three real roots to (4.23) for a small interval of wavenumbers adjacent to $k = 0$. At the onset of instability, the two neutral topographic modes coalesce, and as seen in Fig. 6b, of course, an exponentially growing and decaying pair of topographic waves develop. Eventually as k increases, the high wavenumber cutoff is reached and a pair of neutral topographic waves reemerges. For no parameter values did the planetary wave coalesce with a topographic wave to produce instability.

The most unstable mode occurs at the meridional, or along-slope, wavenumber $k_{\max}$, satisfying

$$\left.\frac{\partial\sigma}{\partial k}\right|_{k=k_{\max}} = 0 \quad \text{and} \quad \sigma_{\max} = \max_{\sigma}[\sigma(k_{\max})], \tag{4.26}$$

for fixed l, β, and γ. The corresponding real phase velocity is denoted $c_{R_{\max}} = \mathrm{Re}\,(c_{\max})$ and the frequency is denoted $\omega_{\max} = k_{\max}|c_{R_{\max}}|$. Figs. 7a,b,c,d are contour plots of $k_{\max}$, $c_{R_{\max}}$, $\omega_{\max}$, and $\sigma_{\max}$, respectively, in the (γ, β) plane for $l = \pi/10$. These figures show that, for fixed γ, the most unstable mode has an increasing wavenumber, decreasing phase speed (but always southward, of course), increasing frequency and decreasing growth rate, for increasing β. There is no value of β such that, for all larger values, the instability does not occur. Thus, while β has a stabilizing effect, it does not, for a sufficiently high value, eliminate the instability of an otherwise unstable mode. The variations that occur with respect to increasing β, for fixed γ, are relatively modest. Based on the nondimensionalizations introduced in section 2, it is possible to characterize the most unstable mode as having an along-slope wavelength on the order of 94 km, an equatorward phase velocity on the order of 3 cm s^{-1} a modal period on the order of 38 days and an e-folding amplification time on the order of 6 days.

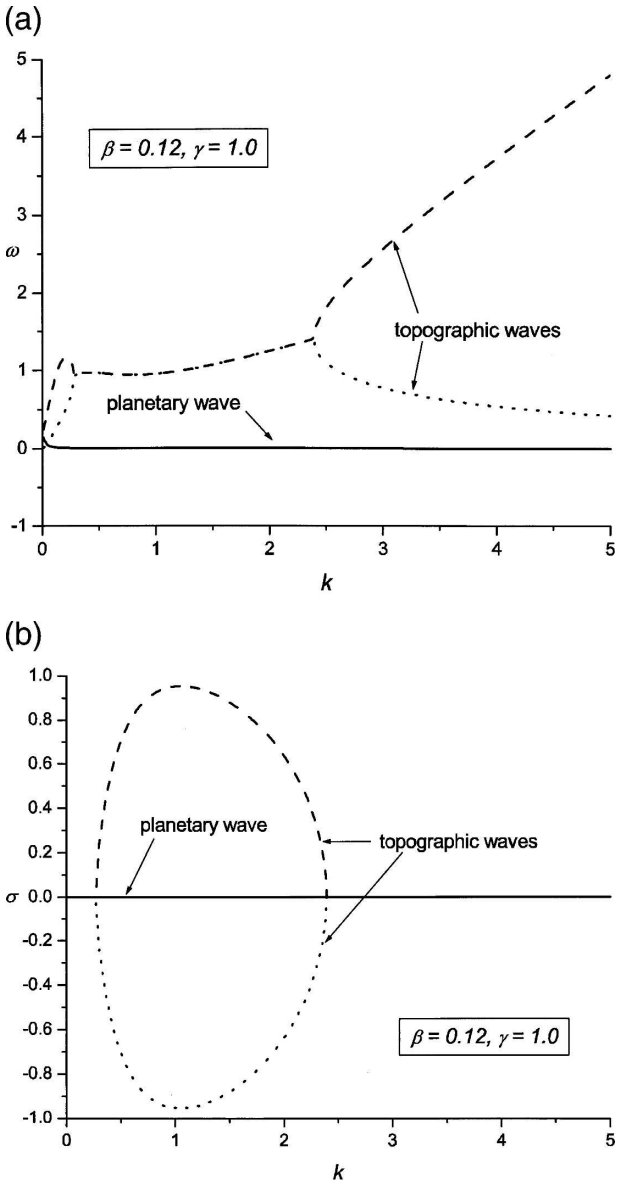

FIG. 6. (a) The modal frequencies $\omega = k\mathrm{Re}(c)$ vs k and (b) the model growth rates $\sigma = k\mathrm{Im}(c)$ vs k, as determined by (4.23), with $l = \pi/10$, $\gamma = 1.0$, and $\beta = 0.12$.

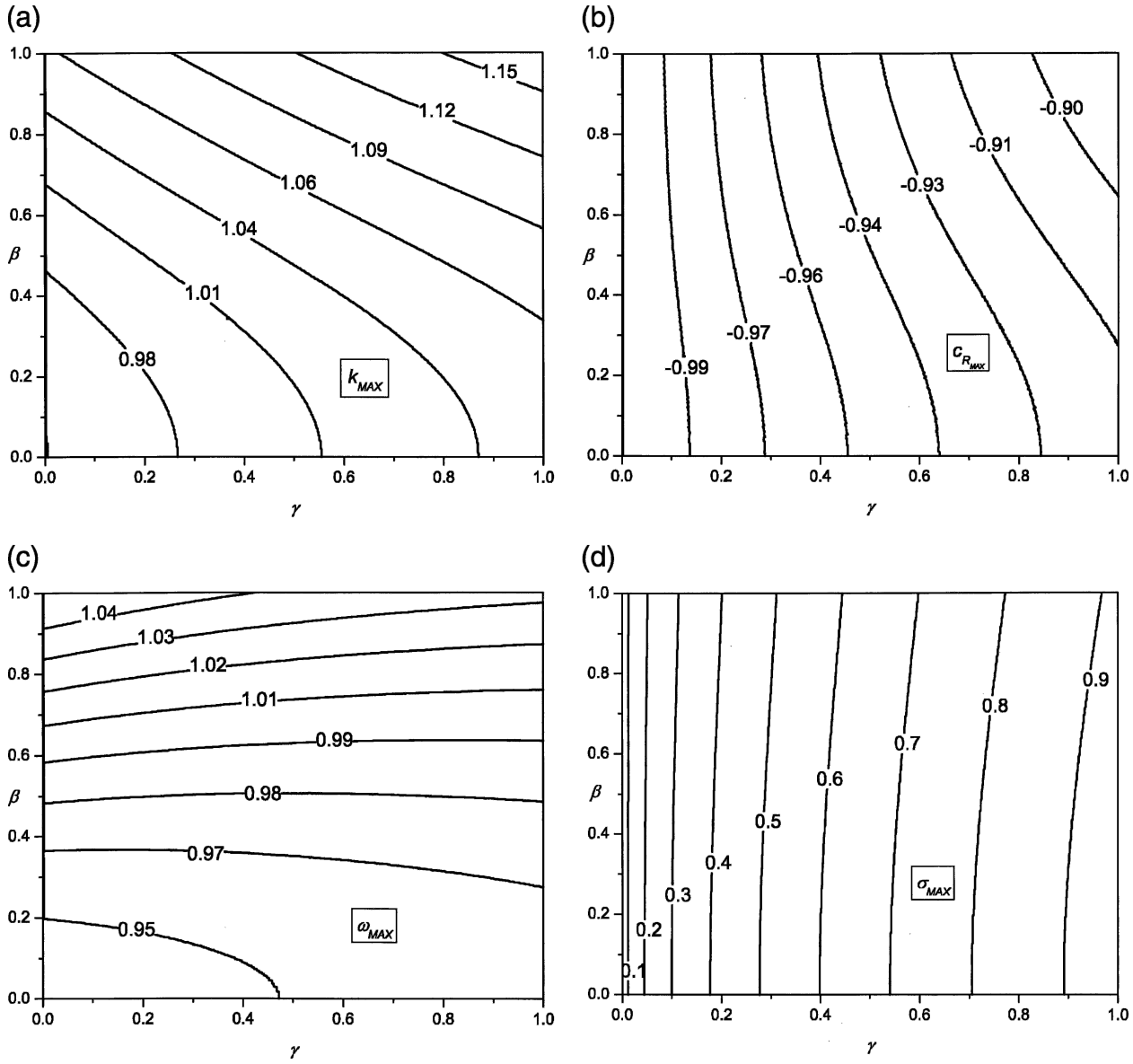

FIG. 7. (a) Contour plot of the meridional, or along-slope, wavenumber of the most unstable mode, $k_{\max}$, in the (γ, β) plane, as determined by (4.23), with $l = \pi/10$. Dimensionally, $k_{\max} = 1.0$ implies a wavelength of about 94 km. (b) Contour plot of the meridional, or along-slope, phase velocity of the most unstable mode, $c_{R_{\max}}$, in the (γ, β) plane, as determined by (4.23), with $l = \pi/10$. Dimensionally, $|c_{R_{\max}}| = 1.0$ implies a phase speed of about 3 cm s^{-1}. (c) Contour plot of the frequency of the most unstable mode, $\omega_{\max}$, in the (γ, β) plane, as determined by (4.23), with $l = \pi/10$. Dimensionally, $\omega_{\max} = 1.0$ implies a period of about 38 days. (d) Contour plot of the growth rate of the most unstable mode, $\sigma_{\max}$, in the (γ, β) plane, as determined by (4.23), with $l = \pi/10$. Dimensionally, $\sigma_{\max} = 1.0$ implies an *e*-folding time of about 6 days.

5. Conclusions

The meridional flow of abyssal currents in a stratified basin with topography and β has been examined. Conceptually, the model examined here describes grounded source-driven meridional abyssal flow over sloping topography as a process that initiates as a Stommel–Arons flow (satisfying a Sverdrup vorticity balance) that then transitions to an inertial topographically steered Nof flow (which is geostrophically balanced) away from the source region, all the while baroclinically interacting with the overlying ocean. The model equations correspond to a three-layer QG–PG model with interlayer mass exchange that conserves the horizontal divergence of the barotropic mass flux (i.e., the unforced, inviscid dynamics is purely baroclinic). The

abyssal-layer PG equations allow for groundings in the height field.

The model has a number of important subdynamical limits within it such as the Nof balance describing topographically steered abyssal flow (Nof 1983), the Stommel–Arons Sverdrup vorticity balance describing the equatorward flow of an abyssal water mass created by a source (Stommel and Arons 1960), the planetary shock wave balance (Anderson and Killworth 1979; Johnson and Willmott 1981; Dewar 1987a; Wright and Willmott 1992; among others) describing the amplitude-β induced isopycnal steepening and westward propagation of abyssal anomalies and, finally, the coupling between the abyssal layer and the overlying ocean that will lead to baroclinic instability (Swaters 1991, 1998).

In the reduced gravity approximation, a new nonlinear steady-state balance was identified that is a combined approximation including both Stommel–Arons source-driven flow and steady or long-time Nof flow over sloping topography, valid for grounded abyssal currents on a midlatitude β plane. It was possible to explicitly solve this model for an abyssal current with upslope and downslope groundings. The thickness of the abyssal current decreases equatorward (although the meridional transport remains constant, i.e., the equatorward speed of the current increases in the equatorward direction) as result of the conservation (away from the source region) of planetary geostrophic potential vorticity.

The baroclinic instability characteristics that the model predicts were examined. In particular, a variational principle is introduced for the baroclinic extension of the hybrid (inertial) Stommel–Arons–Nof solution. This variational principle was exploited to sufficient stability and necessary instability conditions that generalize previous f-plane results. The linear baroclinic instability problem was solved for a constant abyssal current with β and sloping topography present.

This paper presents a theoretical discussion of the baroclinic dynamics of abyssal ocean currents. In a subsequent contribution, a full numerical simulation will be presented for the basin-scale development of source-driven grounded abyssal currents with topography, β, forcing and dissipation parameter values characteristic of the deep western boundary undercurrent in the North Atlantic (in the absence of wind stress). In a further contribution, the interaction of source-driven grounded abyssal currents with the surface-intensified wind-driven circulation (in particular the Gulf Stream) will be described.

Acknowledgments. Preparation of this paper was supported in part by the Natural Sciences and Engineering Research Council of Canada.

APPENDIX

Model Derivation as an Asymptotic Reduction of the Shallow Water Equations

The purpose of this appendix is to briefly summarize the derivation of the nondimensional model as an asymptotic reduction of the three-layer shallow water equations. The underlying dimensional three-layer shallow water equations, in standard notation, from which the model (2.1), (2.2), and (2.3) is derived, are given by

$$(\partial_{t^*} + \mathbf{u}_1^* \cdot \boldsymbol{\nabla}^*)\mathbf{u}_1^* + f\mathbf{e}_3 \times \mathbf{u}_1^* = -\frac{\boldsymbol{\nabla}^*\phi_1^*}{\rho_*} + A_H\Delta^*\mathbf{u}_1^*,$$

$$H_1\boldsymbol{\nabla}^* \cdot \mathbf{u}_1^* = \eta_{t^*}^* + \boldsymbol{\nabla}^* \cdot (\mathbf{u}_1^*\eta^*) - \frac{\boldsymbol{\nabla}^* \times \boldsymbol{\tau}^*}{\rho_* f_0} - \left(\frac{H_1 - \eta^*}{H_1 + H_2 - h^* - h_B^*}\right)Q^*, \tag{A.1}$$

$$(\partial_{t^*} + \mathbf{u}_2^* \cdot \nabla^*)\mathbf{u}_2^* + f\mathbf{e}_3 \times \mathbf{u}_2^* = -\frac{\nabla^*\phi_2^*}{\rho_*} + A_H\Delta^*\mathbf{u}_2^*,$$

$$H_2\nabla^* \cdot \mathbf{u}_2^* = (h^* - \eta^*)_{t^*} + \nabla^* \cdot [\mathbf{u}_2^*(h^* + h_B^* - \eta^*)] + r_2^*\nabla^* \times \mathbf{u}_2^* - \left(\frac{H_2 + \eta^* - h^* - h_B^*}{H_1 + H_2 - h^* - h_B^*}\right)Q^*, \tag{A.2}$$

$$(\partial_{t^*} + \mathbf{u}_3^* \cdot \boldsymbol{\nabla}^*)\mathbf{u}_3^* + f\mathbf{e}_3 \times \mathbf{u}_3^* = -\frac{\boldsymbol{\nabla}^* p^*}{\rho_*},$$

$$h_{t^*}^* + \boldsymbol{\nabla}^* \cdot (\mathbf{u}_3^* h^*) = Q^* + r_3^*\boldsymbol{\nabla}^* \times \mathbf{u}_3^*, \quad \text{and} \tag{A.3}$$

$$\rho_* \tilde{g}\eta^* = \phi_2^* - \phi_1^*, p^* = \phi_2^* + \rho_* g'(h^* + h_B^*). \tag{A.4}$$

The horizontal divergence of the barotropic mass flux is obtained by forming the sum (A.1) + (A.2) + (A.3) (second equation of each) and is given by

$$\nabla^* \cdot [\mathbf{u}_1^*(H_1 - \eta^*) + \mathbf{u}_2^*(H_2 + \eta^* - h^* - h_B^*) + \mathbf{u}_3^* h^*] = -\frac{\nabla^* \times \boldsymbol{\tau}^*}{\rho_* f} + r_2^* \nabla^* \times \mathbf{u}_2^* + r_3^* \nabla^* \times \mathbf{u}_3^*. \tag{A.5}$$

It is important to appreciate that in the unforced, inviscid limit, the horizontal divergence of the barotropic mass flux is zero (and consequently that total volume is conserved with this upwelling/downwelling parameterization). The mass exchange between the abyssal layer and the QG layers is assumed to be instantaneous and distributed in proportion to the individual upper layer volume fractions in such a manner that there is no net mass gain or loss. The horizontal divergence of the barotropic mass transport is forced only by wind stress and bottom friction. The unforced, inviscid dynamics of the model is, therefore, purely baroclinic.

The nondimensional equations are obtained by substituting the scalings, given by

$$(x^*, y^*) = L(x, y), \qquad t^* = \frac{Lf_0}{s^* g'} t, \qquad h^* = s^* L h,$$
$$\mathbf{u}_{1,2,3}^* = U_* \mathbf{u}_{1,2,3}, \qquad p^* = \rho_* L g' s^* p,$$
$$\phi_{1,2}^* = \rho_* L f_0 U_* \phi_{1,2}, \quad \eta^* = \frac{f_0 U_* L}{\tilde{g}} \eta,$$
$$Q^* = \frac{(s^*)^2 g'}{f_0} Q, \qquad \boldsymbol{\tau}^* = \Upsilon^* \boldsymbol{\tau}, \quad \text{and} \quad h_B^* = s^* L h_B, \tag{A.6}$$

into (A.1), (A.2), (A.3), and (A.4), yielding

$$s(\partial_t + \mathbf{u}_1 \cdot \nabla)\mathbf{u}_1 + (1 + s\beta y)\mathbf{e}_3 \times \mathbf{u}_1 = -\nabla\phi_1 + \frac{s}{R_e}\Delta\mathbf{u}_1,$$
$$\nabla \cdot \mathbf{u}_1 = s\left\{F_1[\eta_t + \nabla \cdot (\mathbf{u}_1\eta)] - \Upsilon \nabla \times \tau - \frac{F_1}{F_1 + F_2} Q\right\} + O(s^2), \tag{A.7}$$

$$s(\partial_t + \mathbf{u}_2 \cdot \nabla)\mathbf{u}_2 + (1 + s\beta y)\mathbf{e}_3 \times \mathbf{u}_2 = -\nabla\phi_2 + \frac{s}{R_e}\Delta\mathbf{u}_2,$$
$$\nabla \cdot \mathbf{u}_2 = s\left\{(h - F_2\eta)_t + \nabla \cdot [\mathbf{u}_2(h + h_B - F_2\eta)] + r_2 \nabla \times \mathbf{u}_2 - \frac{F_1}{F_1 + F_2} Q\right\} + O(s^2), \tag{A.8}$$

$$s(\partial_t + \mathbf{u}_3 \cdot \nabla)\mathbf{u}_3 + (1 + s\beta y)\mathbf{e}_3 \times \mathbf{u}_3 = -\nabla p, h_t + \nabla \cdot (\mathbf{u}_3 h) = Q + r_3 \nabla \times \mathbf{u}_3, \tag{A.9}$$

$$\eta = \phi_2 - \phi_1, \quad \text{and} \quad p = h + h_B + \phi_2. \tag{A.10}$$

The models (2.1), (2.2), (2.3), and (2.4) are obtained as the $0 < s \ll 1$ limit of (A.7), (A.8), (A.9), and (A.10).

Some of the scalings in may seem a little odd at first. For example, the upper and middle layers' velocities have been scaled by the Nof velocity. This is the correct dynamical scaling assuming a balance between relative vorticity and baroclinic stretching induced by the abyssal layer, that is,

$$\nabla^* \times \mathbf{u}_2^* \approx O\left(\frac{f_0 h^*}{H_2}\right) \Rightarrow \mathbf{u}_2^* \approx O\left(\frac{f_0 s^* L^2}{H_2}\right) = O\left(\frac{s^* g'}{f_0}\right). \tag{A.11}$$

The same scaling has been chosen for $\mathbf{u}_1^*$ since it is assumed that ϕ_1^* and ϕ_2^* scale similarly, and ϕ_2^* is geostrophically scaled. The scaling of the abyssal layer height by s^*L (which is the rise of the topography over

a deformation radius) is a convenience that eliminates the nondimensional interaction parameter introduced by Swaters (1991). The scaling for the up/downwelling parameter has been chosen so that $Q^* \approx O(h_{t^*}^*) = s^{*2}g'/f_0$ and has units of (vertical) velocity.

REFERENCES

Anderson, D., and P. D. Killworth, 1979: Non-linear propagation of long Rossby waves. *Deep-Sea Res.,* **26,** 1033–1050.

Charney, J. G., and G. R. Flierl, 1981: Oceanic analogues of large scale atmospheric motions. *Evolution of Physical Oceanography—Scientific Surveys in Honor of Henry Stommel,* B. A. Warren and C. Wunsch, Eds., MIT Press, 504–548.

Choboter, P. F., and G. E. Swaters, 2000: On the baroclinic instability of axisymmetric rotating gravity currents with bottom slope. *J. Fluid Mech.,* **408,** 149–177.

——, and ——, 2003: Two-layer models of abyssal equator cross flow. *J. Phys. Oceanogr.,* **33,** 1401–1415.

——, and ——, 2004: Shallow water modeling of Antarctic Bottom Water crossing the equator. *J. Geophys. Res.,* **109,** C03038, doi:10.1029/2003JC002048.

de Verdiere, A. C., 1986: On mean flow instabilities within the planetary geostrophic equations. *J. Phys. Oceanogr.,* **16,** 1981–1984.

Dewar, W. K., 1987a: Planetary shock waves. *J. Phys. Oceanogr.,* **17,** 470–482.

——, 1987b: Ventilating warm rings: Theory and energetics. *J. Phys. Oceanogr.,* **17,** 2219–2231.

——, 1988a: Ventilating warm rings: Structure and model evaluation. *J. Phys. Oceanogr.,* **18,** 552–564.

——, 1988b: Ventilating β-plane lenses. *J. Phys. Oceanogr.,* **18,** 1193–1201.

Edwards, C. A., and J. Pedlosky, 1998a: Dynamics of nonlinear cross-equatorial flow. Part I: Potential vorticity transformation. *J. Phys. Oceanogr.,* **28,** 2382–2406.

——, and ——, 1998b: Dynamics of nonlinear cross-equatorial flow. Part II: The tropically enhanced instability of the western boundary current. *J. Phys. Oceanogr.,* **28,** 2407–2417.

Edwards, N. R., A. J. Willmott, and P. D. Killworth, 1998: On the role of topography and wind stress on the stability of the thermohaline circulation. *J. Phys. Oceanogr.,* **28,** 756–778.

Etling, D., F. Gelhardt, U. Schrader, F. Brennecke, G. Kühn, G. Chabert d'Hieres, and H. Didelle, 2000: Experiments with density currents on a sloping bottom in a rotating fluid. *Dyn. Atmos. Oceans,* **31,** 139–164.

Flierl, G. R., 1984: Rossby wave radiation from a strongly nonlinear warm eddy. *J. Phys. Oceanogr.,* **14,** 47–58.

Griffiths, R. W., P. D. Killworth, and M. Stern, 1982: Ageostrophic instability of ocean currents. *J. Fluid Mech.,* **117,** 343–377.

Ha, S. J., and G. E. Swaters, 2006: Finite-amplitude baroclinic instability of time-varying abyssal currents. *J. Phys. Oceanogr.,* **36,** 122–139.

Holland, W. R., 1978: The role of mesoscale eddies in the general circulation of the ocean—Numerical experiments using a wind-driven quasi-geostrophic model. *J. Phys. Oceanogr.,* **8,** 363–392.

Jiang, L., and R. W. Garwood Jr., 1996: Three dimensional simulations of overflows on continental slopes. *J. Phys. Oceanogr.,* **26,** 1214–1233.

Johnson, J. A., and A. J. Willmott, 1981: An unsteady wind-driven ocean circulation model. *Dyn. Atmos. Oceans,* **6,** 1–27.

Jungclaus, J. H., J. Hauser, and R. H. Käse, 2001: Cyclogenesis in the Denmark Strait overflow plume. *J. Phys. Oceanogr.,* **31,** 3214–3229.

Karsten, R. H., and G. E. Swaters, 1999: A unified asymptotic derivation of two-layer, frontal geostrophic models including planetary sphericity and variable topography. *Phys. Fluids,* **11,** 2583–2597.

——, and ——, 2000: Nonlinear effects in two-layer large-amplitude geostrophic dynamics. Part 2. The weak-beta case. *J. Fluid Mech.,* **412,** 161–196.

——, ——, and R. E. Thomson, 1995: Stability characteristics of deep-water replacement in the Strait of Georgia. *J. Phys. Oceanogr.,* **25,** 2391–2403.

Katsman, C. A., S. S. Drijfhout, and H. A. Dijkstra, 2001: The interaction of a deep western boundary current and the wind-driven gyres as a cause for low-frequency variability. *J. Phys. Oceanogr.,* **31,** 2321–2339.

Kawase, M., 1987: Establishment of deep ocean circulation by deep-water production. *J. Phys. Oceanogr.,* **17,** 2294–2317.

——, and D. Straub, 1991: Spinup of source-driven circulation in an abyssal basin in the presence of bottom topography. *J. Phys. Oceanogr.,* **21,** 1501–1514.

Lane-Serff, G. F., and P. Baines, 1998: Eddy formation by dense flows on slopes in a rotating fluid. *J. Fluid Mech.,* **363,** 229–252.

LeBlond, P. H., H. Ma, F. Doherty, and S. Pond, 1991: Deep and intermediate water replacement in the Strait of Georgia. *Atmos.–Ocean,* **29,** 288–312.

Longuet-Higgins, M. S., 1965: Planetary waves on a rotating sphere, II. *Proc. Roy. Soc. London A,* **284,** 40–68.

Masson, D., 2002: Deep water renewal in the Strait of Georgia. *Estuarine, Coastal Shelf Sci.,* **54,** 115–126.

Mooney, C. J., and G. E. Swaters, 1996: Finite amplitude baroclinic instability of a mesoscale gravity current in a channel. *Geophys. Astrophys. Fluid Dyn.,* **82,** 173–205.

Nof, D., 1983: The translation of isolated cold eddies on a sloping bottom. *Deep-Sea Res.,* **30,** 171–182.

——, and S. Borisov, 1998: Inter-hemispheric oceanic exchange. *Quart. J. Roy. Meteor. Soc.,* **124,** 2829–2866.

Pavec, M., X. Carton, and G. Swaters, 2005: Baroclinic instability of frontal geostrophic currents over a slope. *J. Phys. Oceanogr.,* **35,** 911–918.

Pedlosky, J., 1984: The equations for geostrophic flow in the ocean. *J. Phys. Oceanogr.,* **14,** 448–455.

——, 1987: *Geophysical Fluid Dynamics.* 2d ed. Springer-Verlag, 710 pp.

——, 1996: *Ocean Circulation Theory.* Springer-Verlag, 453 pp.

Poulin, F. J., and G. E. Swaters, 1999: Sub-inertial dynamics of density-driven flows in a continuously stratified fluid on a sloping bottom. I. Model derivation and stability conditions. *Proc. Roy. Soc. London A,* **455,** 2281–2304.

Reszka, M. K., G. E. Swaters, and B. R. Sutherland, 2002: Instability of abyssal currents in a continuously stratified ocean with bottom topography. *J. Phys. Oceanogr.,* **32,** 3528–3550.

Rhines, P. B., 1989: Deep planetary circulation and topography: Simple models of midocean flows. *J. Phys. Oceanogr.,* **19,** 1449–1470.

Richardson, P. L., 1977: On the crossover between the Gulf Stream and the Western Boundary Undercurrent. *Deep-Sea Res.,* **24,** 139–159.

Samelson, R. M., 1998: Large-scale circulation with locally enhanced vertical mixing. *J. Phys. Oceanogr.,* **28,** 712–726.

——, and G. K. Vallis, 1997: A simple frictional and diffusion scheme for planetary geostrophic basin models. *J. Phys. Oceanogr.,* **27,** 186–194.

Speer, K. E., and M. S. McCartney, 1992: Bottom Water circulation in the western North Atlantic. *J. Phys. Oceanogr.,* **22,** 83–92.

——, E. Tiperman, and Y. Feliks, 1993: Topography and grounding in an simple bottom layer model. *J. Geophys. Res.,* **98,** 2667–2682.

Stephens, J. C., and D. P. Marshall, 2000: Dynamical pathways of Antarctic Bottom Water in the Atlantic. *J. Phys. Oceanogr.,* **30,** 622–640.

Stommel, H., and A. B. Arons, 1960: On the abyssal circulation of the World Ocean - I. Stationary flow patterns on a sphere. *Deep-Sea Res.,* **6,** 140–154.

Straub, D. N., P. D. Killworth, and M. Kawase, 1993: A simple model of mass-driven abyssal circulation over general bottom topography. *J. Phys. Oceanogr.,* **23,** 1454–1469.

Sutherland, B. R., J. Nault, K. Yewchuk, and G. E. Swaters, 2004: Rotating dense currents on a slope. Part 1. Stability. *J. Fluid Mech.,* **508,** 241–264.

Swaters, G. E., 1991: On the baroclinic instability of cold-core coupled density fronts on sloping continental shelf. *J. Fluid Mech.,* **224,** 361–382.

——, 1993: Nonlinear stability of intermediate baroclinic flow on a sloping bottom. *Proc. Roy. Soc. London A,* **442,** 249–272.

——, 1998: Numerical simulations of the baroclinic dynamics of density-driven coupled fronts and eddies on a sloping bottom. *J. Geophys. Res.,* **103,** 2945–2961.

——, 2000: *Introduction to Hamiltonian Fluid Dynamics and Stability Theory.* Chapman and Hall, 274 pp.

——, 2003: Baroclinic characteristics of frictionally destabilized abyssal overflows. *J. Fluid Mech.,* **489,** 349–379.

——, 2006: On the meridional flow of source-driven abyssal currents in a stratified basin with topography. Part II. Numerical simulation. *J. Phys. Oceanogr.,* **36,** 356–375.

——, and G. R. Flierl, 1991: Dynamics of ventilated coherent cold eddies on a sloping bottom. *J. Fluid Mech.,* **223,** 565–587.

Willmott, A. J., N. R. Edwards, and D. G. Wright, 1996: Abyssal circulation in a circumpolar basin driven by discrete sources of buoyancy. *J. Phys. Oceanogr.,* **26,** 49–64.

Wright, D. G., and A. J. Willmott, 1992: Buoyancy driven abyssal circulation in a circumpolar basin. *J. Phys. Oceanogr.,* **22,** 139–154.